Supporting Information for

Environ. Sci. Technol.

Electrochemical analysis of changes in iron oxide reducibility during abiotic ferrihydrite transformation into goethite and magnetite

Meret Aeppli[1], Ralf Kaegi[2], Ruben Kretzschmar[1],
Andreas Voegelin[2], Thomas B. Hofstetter[1,2*], and Michael Sander[*,1]

[1]Institute of Biogeochemistry and Pollutant Dynamics, ETH Zurich, CHN, 8092 Zurich, Switzerland

[2]Swiss Federal Institute of Aquatic Science and Technology (Eawag), 8600 Duebendorf, Switzerland

[*]Corresponding authors:
thomas.hofstetter@eawag.ch
phone +41 58 765 50 76, fax +41 58 765 58 02
michael.sander@env.ethz.ch
phone +41 44 632 83 14, fax +41 44 632 11 22

54 Pages, 32 Figures, 7 Tables

Contents

S1 Chemicals

3-(*N*-morpholino)propanesulfonic acid (MOPS) was purchased from Sigma. 1,1′- ethylene 2,2′-bipyridyl dibromide (diquat, 99.5%), acetic acid, ammonium fluoride, nitric acid, iron(III) nitrate nonahydrate, and iron(II) chloride tetrahydrate were purchased from Sigma-Aldrich. 1,10-phenanthroline hydrochloride monohydrate, 2-(*N*-morpholino)ethanesulfonic acid (MES), potassium hydroxide, hydrochloric acid, and ammonium acetate were purchased from Merck. Hydroxylamine hydrochloride was purchased from Fluka.

S2 Setup of transformation experiments, preparation and analysis of samples

Figure S1 shows a schematic illustration of the setup of the transformation experiments as well as the preparation steps and analyses of suspension aliquots sampled over the course of the ferrihydrite transformations. In the transformation experiments, we first set the pH of the ferrihydrite suspension to the desired value using the automated pH titrator. We subsequently initiated the phase transformation by adding Fe^{2+} from a concentrated $FeCl_2$ stock solution (200 mM, at pH 6.5 in order to avoid precipitate formation in the stock which would have occurred at higher pH) to the ferrihydrite suspension. The Fe^{2+} addition resulted in a drop of the solution pH in the reactors to values $<$ pH 6 in all transformation experiments. We rapidly titrated the pH back to the desired values using the pH titrator (at most within 30 min of Fe^{2+} addition; see Section S4). Over the entire course of the transformation, the release of H^+ was continuously monitored by pH measurements and compensated by automated titration of 70 mM KOH to maintain a constant pH in the reactors. At selected time points, we withdrew 7 mL suspension aliquots from the reactors using plastic syringes, followed by characterization the iron oxides in these aliquots by X-ray diffraction (XRD), electron microscopy (EM) and mediated electrochemical reduction (MER), as described in materials and methods. We terminated the transformation experiments once XRD analyses showed no further transformation of the iron oxides. The total duration of the transformation experiments varied between 24 h at pH 7.50, 5 mM Fe^{2+} and 720 h at pH 6.75, 5 mM Fe^{2+}.

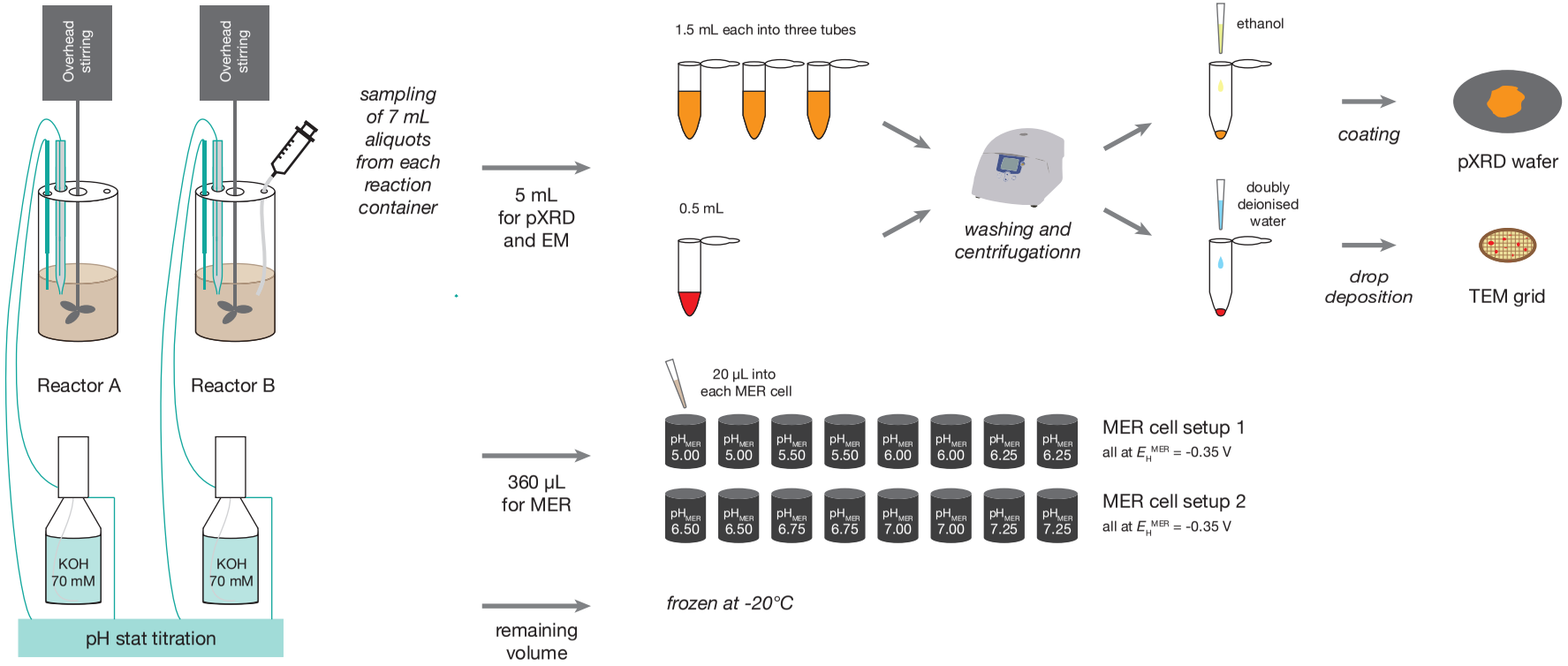

Figure S1 Schematic illustration of the experimental setup of the ferrihydrite transformation experiments and the preparation of aliquots sampled over the course of the transformation for X-ray diffraction (XRD) analysis, electron microscopy (EM) imaging, and mediated electrochemical reduction (MER). Duplicate reactors A and B each containing an initial volume of ferrihydrite suspension of 400 mL (10 mM Fe^{III}) were continuously stirred by overhead stirrers and were connected to an automated pH-stat titrator. The pH in the suspension was continuously measured and was kept constant by addition of base (KOH, 70 mM). Over the course of the transformation, aliquots of 7 mL were repeatedly sampled from each of the two reactors using a plastic syringe. Of these 7 mL, 4.5 mL were used for XRD, 0.5 mL for EM, 0.36 mL for MER, and the remaining volume was frozen. Sample aliquots for XRD and EM analyses were washed with doubly deionised water (DDI), pooled if required, and centrifuged. The XRD sample was prepared by suspending the resulting iron oxide pellet in ethanol and coating the ethanolic suspension onto an XRD slide. The EM sample was prepared by drop depositing the iron oxide pellet re-suspended in DDI onto a TEM grid. Sample aliquots for MER were directly added to electrochemical cells (two setups each consisting of 8 independent cells) that were pre-equilibrated at $E_H^{MER} = -0.35$ V and contained pH-buffered solutions (at pH_{MER} 5.00 to 7.25 as illustrated on the plot) and the electron transfer mediator compound diquat (final concentration of reduced diquat of 0.255 mM in each electrochemical cell).

S3 Ferrihydrite synthesis

Six-line ferrihydrite was synthesised according to Schwertmann and Cornell[1]. In brief, 6 g $Fe(NO_3)_3 \cdot 9H_2O$ were added to 0.6 L of 75°C warm, doubly deionised water (DDI). The suspension was shaken vigorously, placed in an oven at 75°C for 10 min, before being rapidly cooled on ice, followed by dialysis (SpectraPor 7, 10 kD MWCO) of the ferrihydrite suspension for 5 d to remove electrolytes.

S4 pH-stat titration of ferrihydrite transformation experiments

S4.1 Base titration curves during ferrihydrite transformation

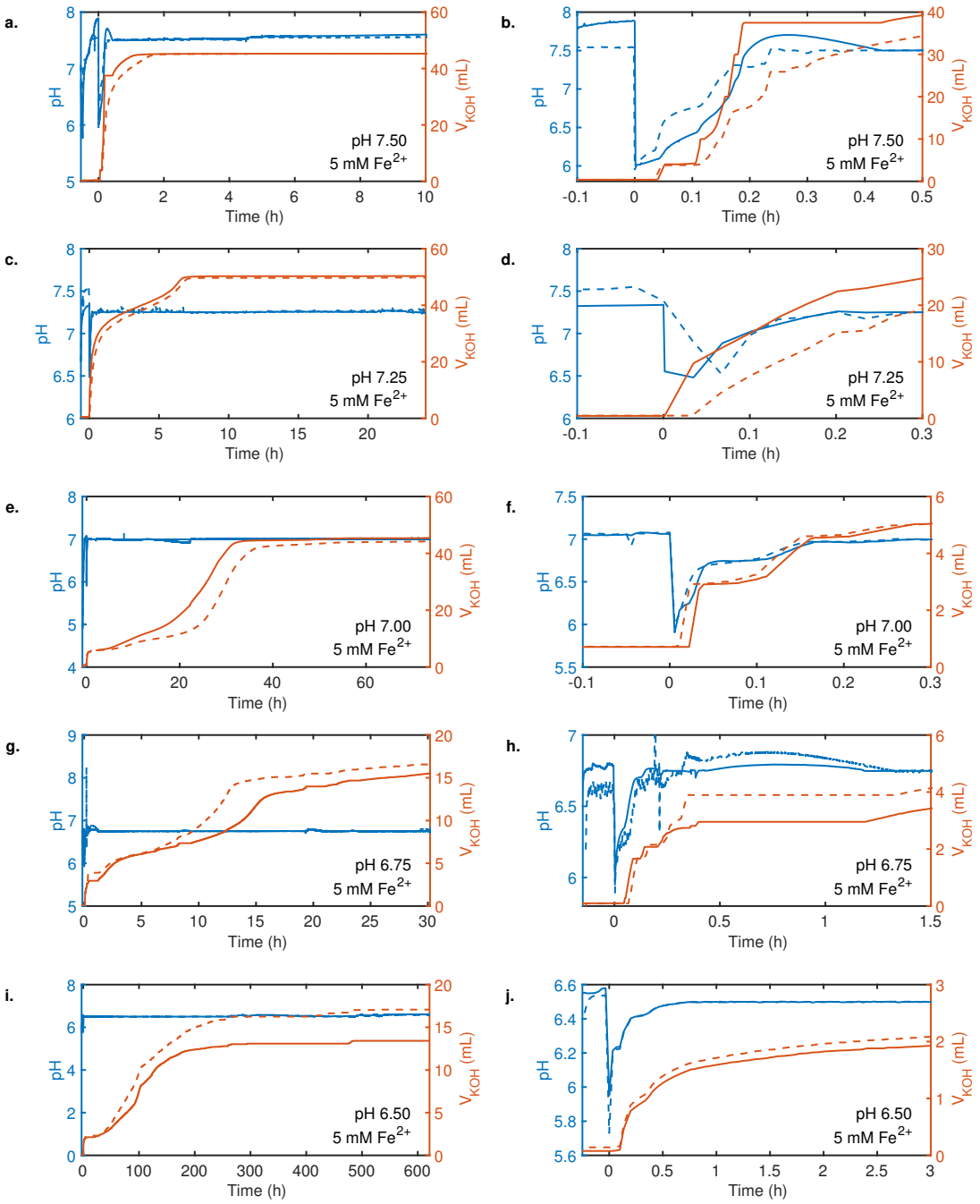

Figure S2 Changes in solution pH and titrated base volume during ferrihydrite transformation experiments at pH 7.50 (**a.**,**b.**), pH 7.25 (**c.**,**d.**), pH 7.00 (**e.**,**f.**), pH 6.75 (**g.**,**h.**), and pH 6.50 (**i.**,**j.**), all at an initial concentration of 5 mM Fe^{2+}. The left y axes shows the pH in the iron oxide suspension and the right y axis the volume of KOH (70 mM) added to the iron oxide suspension. Solid and dashed lines represent reactors A and B, respectively. Panels b., d., f., h., and j. present a closer view on the initial changes in solution pH and volume of titrated base before and after Fe^{2+} addition at $t = 0$ h.

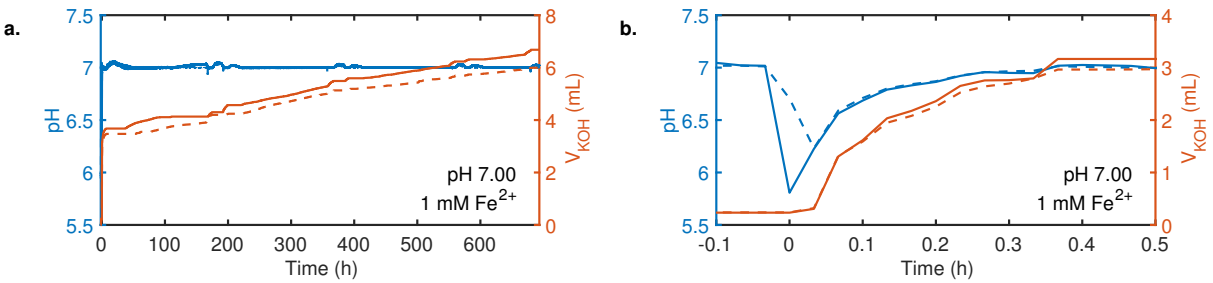

Figure S3 Changes in solution pH and titrated base volume during ferrihydrite transformation experiments at pH 7.00 and at an initial concentration of 1 mM Fe^{2+}. The left y axes in **a.** and **b.** show the pH in the iron oxide suspension and the right y axis the volume of KOH (70 mM) added to the iron oxide suspension. Solid and dashed lines represent reactors A and B, respectively. Panel b. presents a closer view on the initial changes in solution pH and volume of titrated base in before and after Fe^{2+} addition at $t = 0$ h.

S5 Control ferrihydrite transformation experiment without added ferrous iron

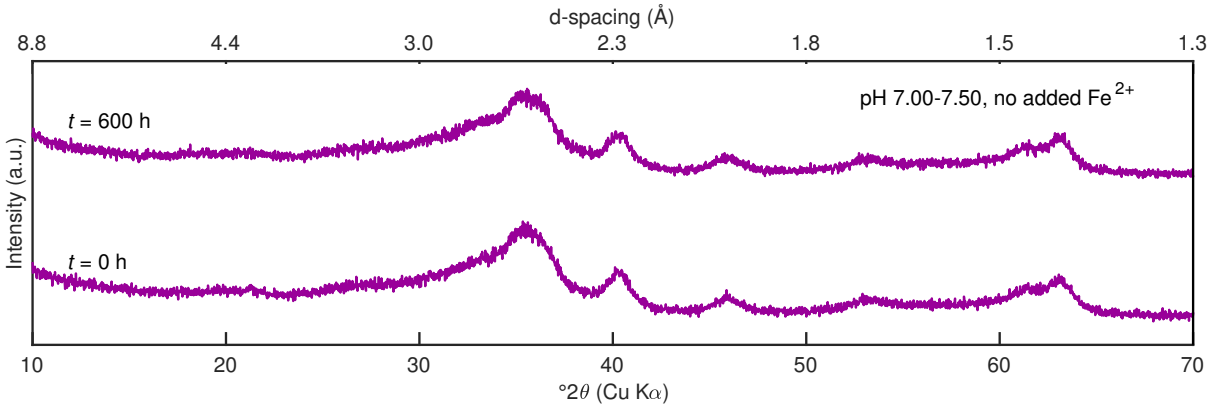

Figure S4 X-ray diffractograms obtained at the beginning (t = 0 h, purple) and the end (t = 600 h) of the ferrihydrite transformation control experiment conducted in the absence of added Fe^{2+}. No transformation of ferrihydrite into more crystalline iron oxide phases was observed.

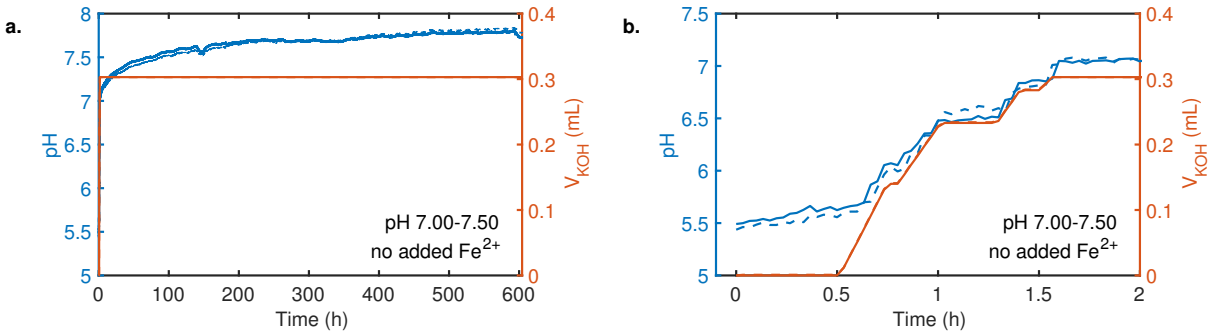

Figure S5 Changes in solution pH and titrated base volume during the ferrihydrite transformation control experiment in the absence of added Fe^{2+} at pH 7.0−7.5. The left y axes in **a.** and **b.** show the pH in the iron oxide suspension and the right y axis the volume of KOH (70 mM) added to the iron oxide suspension. Solid and dashed lines represent reactors A and B, respectively. Panel b. presents a closer view on the initial changes in solution pH and volume of titrated base during the first 2 h of the experiment. Note that the pH of the ferrihydrite suspension increased from 7.00 to >7.50 over the course of 600 h.

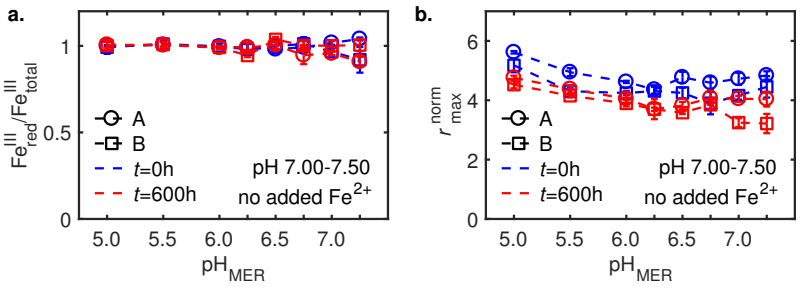

Figure S6 Characterization of iron oxide reactivity towards reduction during the ferrihydrite control experiment in the absence of added Fe^{2+}. Reducible fractions of ferrihydrite-Fe^{III} ($Fe^{III}_{red}/Fe^{III}_{oxide}$, **a.**) and normalized maximum rates of iron oxide reduction (r^{norm}_{max} [$mmol_{e^-}$ $mol_{Fe^{III}}{}^{-1}$ s^{-1}], **b.**) were determined in mediated electrochemical reduction (MER) at the beginning (t = 0h, blue) and end (t = 600 h, red) of the control experiment. Results are shown for duplicate reactors A (circles) and B (squares). MER measurements were performed at pH_{MER} = 5.00 to 7.25, all at E^{MER}_{H}=−0.35 V. $Fe^{III}_{red}/Fe^{III}_{oxide}$ and r^{norm}_{max} were determined as described in the materials and methods section in the main manuscript.

S6 Iron concentrations at the end of each transformation experiment

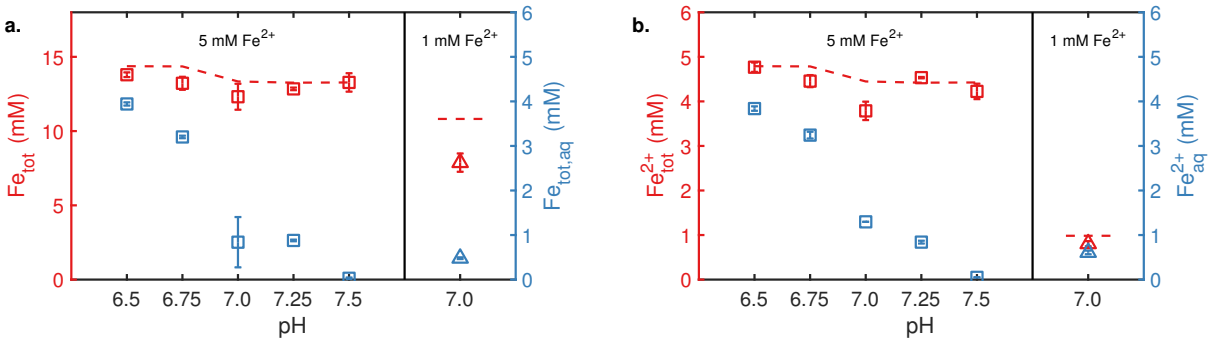

Figure S7 Iron concentrations in the iron oxide suspensions at the end of each ferrihydrite transformation experiment as a function of the solution pH during the transformation experiment. Fe_{tot} (**a.**) and Fe^{2+}_{tot} concentrations (**b.**) were determined using the phenanthroline assay[2] on unfiltered (left y-axes) and on 0.22 μm-filtered samples (labelled 'aq', right y-axes). Dashed red lines depict the calculated concentrations of Fe_{tot} and Fe^{2+}_{tot} based on the removal of iron oxide suspension aliquots for analysis and the addition of base during ferrihydrite transformation experiments.

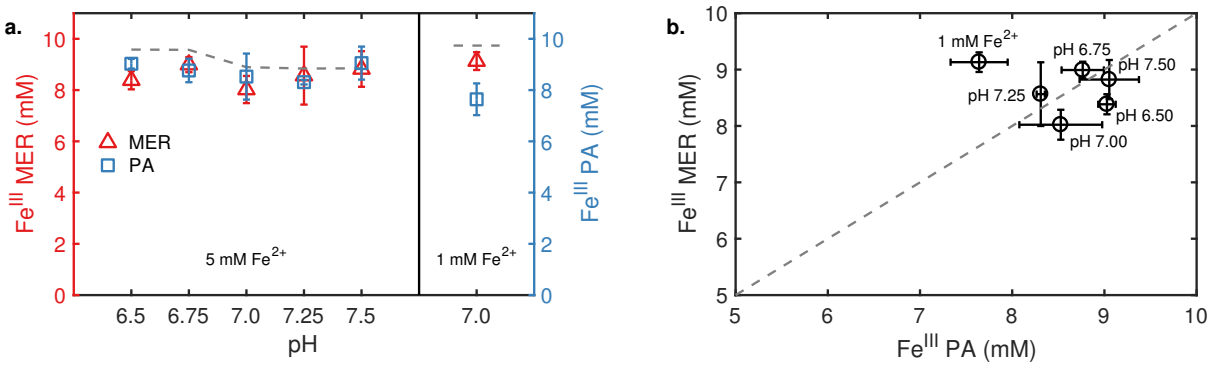

Figure S8 Fe^{III} concentrations in the iron oxide suspensions at the end of each ferrihydrite transformation experiment as measured in mediated electrochemical reduction (MER) at pH_{MER} = 5.0 to 6.5 (E_H^{MER}=−0.35 V) and using the phenanthroline assay (PA)[2]. **a.** Fe^{III} concentrations as a function of the pH of the transformation experiment. Dashed gray lines depict the calculated concentrations of Fe_{tot} and Fe^{2+}_{tot} based on the removal of iron oxide suspension aliquots for analysis and the addition of base during ferrihydrite transformation experiments. **b.** Comparison between Fe^{III} concentrations determined by MER and PA. The individual data points are labelled with the pH (for transformation experiments at constant Fe^{2+} concentration of 5 mM) or Fe^{2+} concentration (for the transformation experiment at pH 7.00 at lower Fe^{2+} concentration of 1 mM) of the respective transformation experiments at the end of which the concentrations were determined.

S7 Specific surface areas of ferrihydrite transformation end-products

Table S1 Specific surface areas (SSA) of the end-products of the ferrihydrite transformation experiments as determined by N_2-BET measurements. Specific surface areas are reported for duplicate reactors A and B in transformation experiments at pH_{trans} 6.5−7.5 (5 mM Fe^{2+}) and at 1 mM Fe^{2+} (pH_{trans} 7.0), as well as for the end-products of the control experiment in the absence of added Fe^{2+} (see Section S5 for details). SSA of the iron oxides in the transformation experiment at pH_{trans} 6.75 could not be determined because the available mass of iron oxide powder was to small for N_2-BET analysis. We note that the relatively large deviation in iron oxide SSA between duplicate reactors in the transformation experiment at pH_{trans} of 7.50 likely was the result of faster transformation of ferrihydrite in reactor A, resulting in smaller magnetite particles (Figure S23g,h) and thus higher SSA, as compared to the slower transformation in reactor B that resulted in larger magnetite particles. Faster ferrihydrite transformation in reactor A was likely caused by the slight overshoot in solution pH during base titration in this reactor (maximum pH of 7.89 in reactor A compared to maximum pH of 7.59 in reactor B, FigureS2a,b.SSA of two batches of ferrihydrite synthesized according to the same procedure (Section S3) as the ferrihydrite used in the transformation experiments were 206.2 and 220.6 m^2g^{-1}. We used the average of these two values to calculate H^+ release during ferrihydrite transformations as described in Section S12.

pH_{trans}	Initial Fe^{2+} concentration (mM)	Reactor	Time (h)	Specific surface area (m^2g^{-1})
6.50	5	A	624	3.8
6.50	5	B	624	2.9
7.00	5	A	53	36.8
7.00	5	B	53	36.5
7.25	5	A	23	41.7
7.25	5	B	23	41.1
7.50	5	A	22	43.5
7.50	5	B	22	19.3
7.00	1	A	672	16.7
7.00	1	B	672	18.2
7.00	-	A	600	101.8
7.00	-	B	600	104.5

S8 X-ray diffraction analysis

S8.1 Calibration of ferrihydrite as PONKCS phase

We calibrated ferrihydrite as 'partial or no known crystal structure' (PONKCS) phaseScarlett and Madsen[3]. To this end, we first recorded X-ray diffractograms of the initial ferrihydrite as freeze-dried powder in a standard sample holder with and without 33 wt% crystalline Al_2O_3 (Fluka, product code 06285) as internal standard (Figure S9). We then fitted the measured diffractogram of ferrihydrite as hkl-phase with fixed cell parameters (space group Fm-3m, a=35 Å) and freely fitted peak intensities. We subsequently fixed the peak intensities and used the resulting fit together with a structure file for corundum (American Mineralogist Crystal Structure Database, 0010593.cif) to fit the diffractogram of ferrihydrite with 33 wt% corundum. Based on this fit, we determined the hkl-cell mass for ferrihydrite and thereby obtained a calibrated hkl-phase. We subsequently used this calibrated hkl-phase together with structure files for goethite (Inorganic Crystal Structure Database, FIZ Karlsruhe (ICSD), ICSD239321.cif), magnetite (ICSD26410.cif), siderite (ICSD169789.cif) and lepidocrocite (ICSD93948.cif) in Rietveld fitting of sample diffractograms.

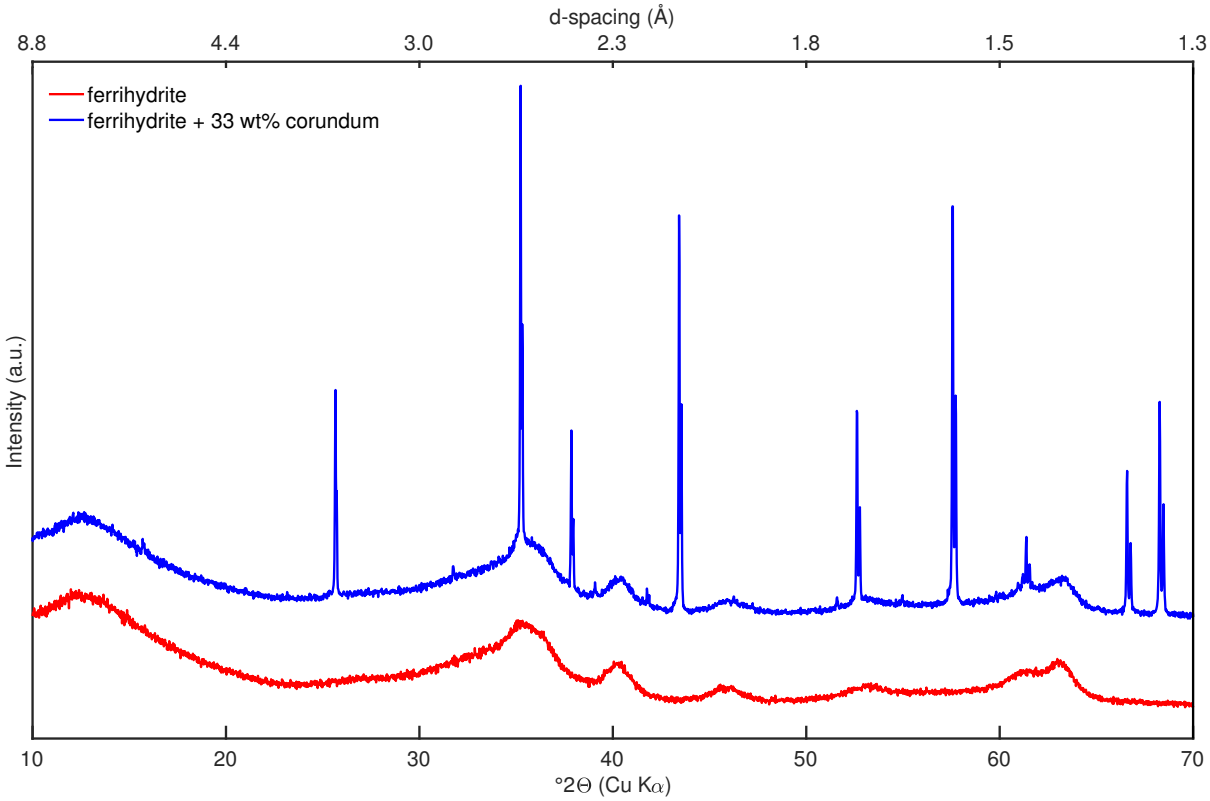

Figure S9 X-ray diffractograms of pure ferrihydrite (red) and ferrihydrite with 33 wt% corundum as internal standard (blue) that were used for the calibration of ferrihydrite as PONKCS phase (see text for details).

We verified accurate quantification of ferrihydrite mass fractions using the PONKC by analyzing ferrihydrite-goethite and ferrihydrite-magnetite mixtures with known mass fractions of

each iron oxide. Iron oxide mixtures were prepared from freeze-dried ferrihydrite powder (synthesized as described in Section S3), goethite powder (Bayferrox 910) or magnetite powder (mknano) by milling the powders, suspending them in 100% ethanol and depositing them on onto zero background Si(510) slides (Siltronix). The XRD measurements were performed as described in materials and methods with the exception that ferrihydrite-magnetite mixtures were measured under oxic conditions (i.e., in the absence of the dome-like X-ray transparent cap).

Rietveld fitting of ferrihydrite-goethite mixtures was performed from 20 to 70°2θ. For the fitting, we fixed the background and goethite cell parameters (a, b, c) to the values fitted on a pure goethite sample. For ferrihydrite-magnetite mixtures, we performed Rietveld fitting from 22 to 70°2θ.

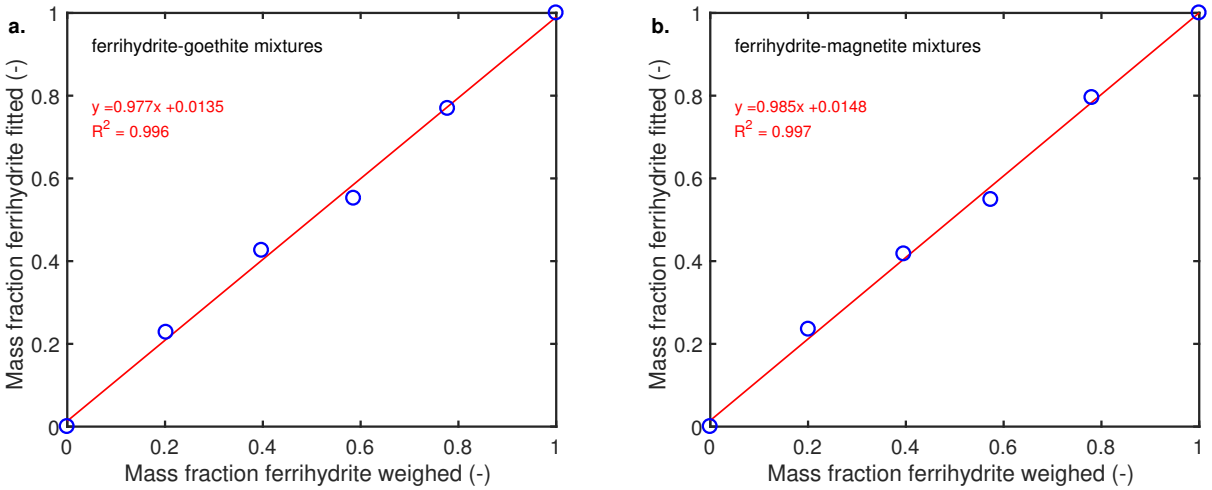

Figure S10 Rietveld fitting of X-ray diffractograms of ferrihydrite-goethite (**a.**) and ferrihydrite-magnetite (**b.**) mixtures of known iron oxide mass fractions. Comparison between fitted ferrihydrite mass fractions (y axes) and weighed ferrihydrite mass fractions (x axes). The solid red lines represent linear fits to the data and the resulting fitting parameters are shown on the plot.

S8.2 X-ray diffractograms of iron oxides during ferrihydrite transformation

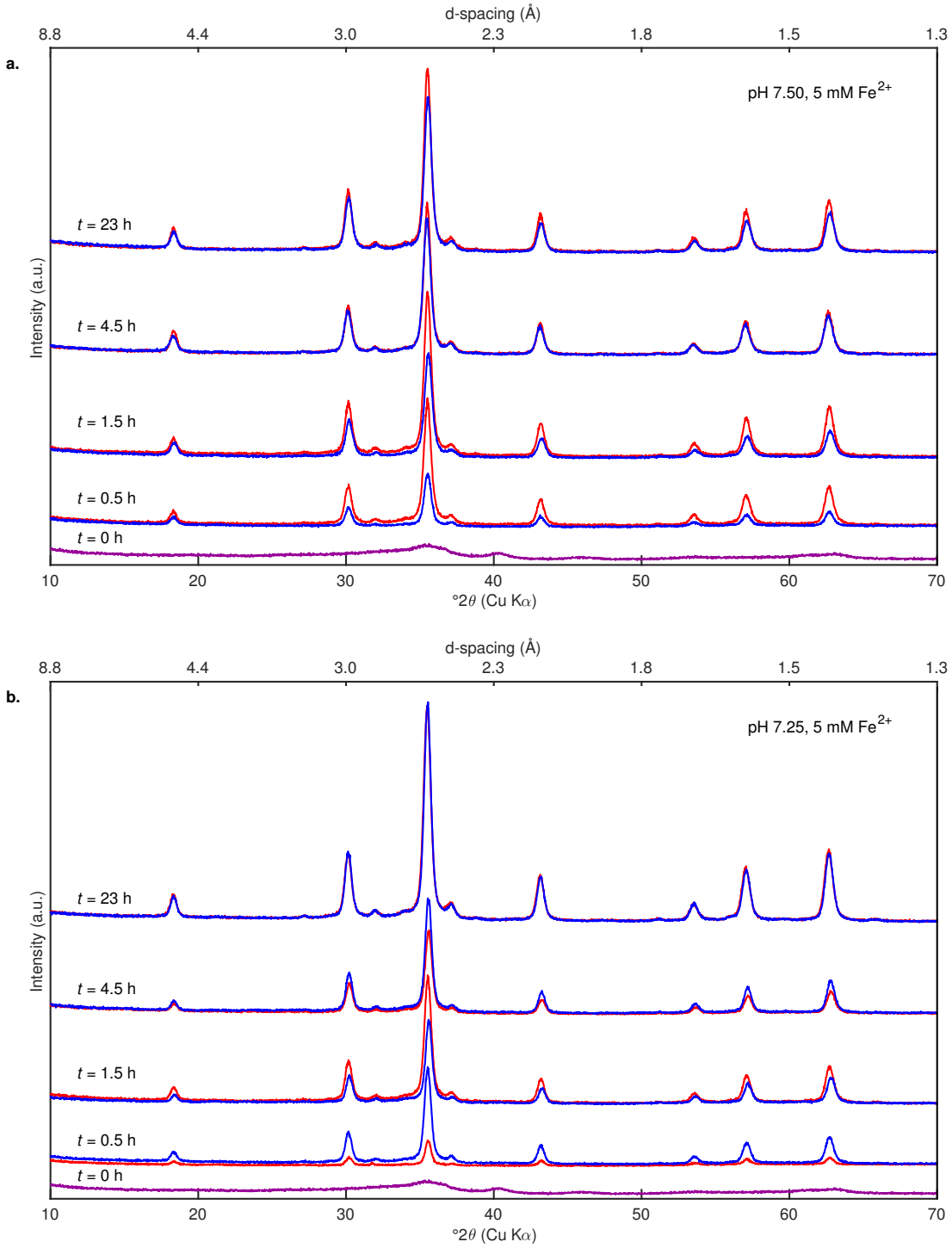

Figure S11 Selected X-ray diffractograms obtained during ferrihydrite transformation experiments at initial Fe^{2+} concentrations of 5 mM at pH 7.50 (**a.**) and pH 7.25 (**b.**). Sample aliquots were removed from duplicate reactors A (red) and B (blue) at selected time points (t) during the transformations as labelled on the plot.

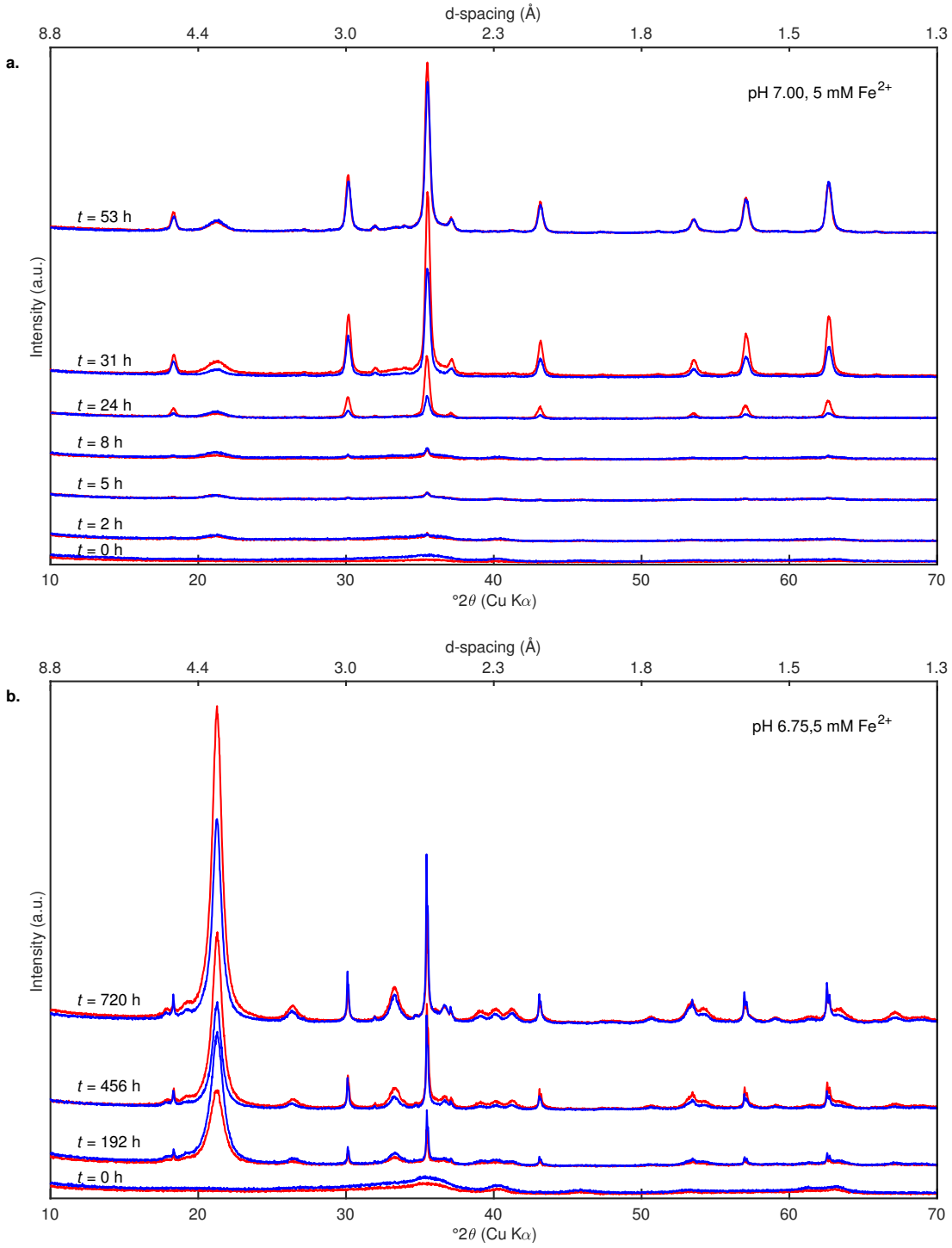

Figure S12 Selected X-ray diffractograms obtained during ferrihydrite transformation experiments at initial Fe^{2+} concentrations of 5 mM at pH 7.00 (**a.**) and pH 6.75 (**b.**). Sample aliquots were removed from duplicate reactors A (red) and B (blue) at selected time points (t) during the transformations as labelled on the plot.

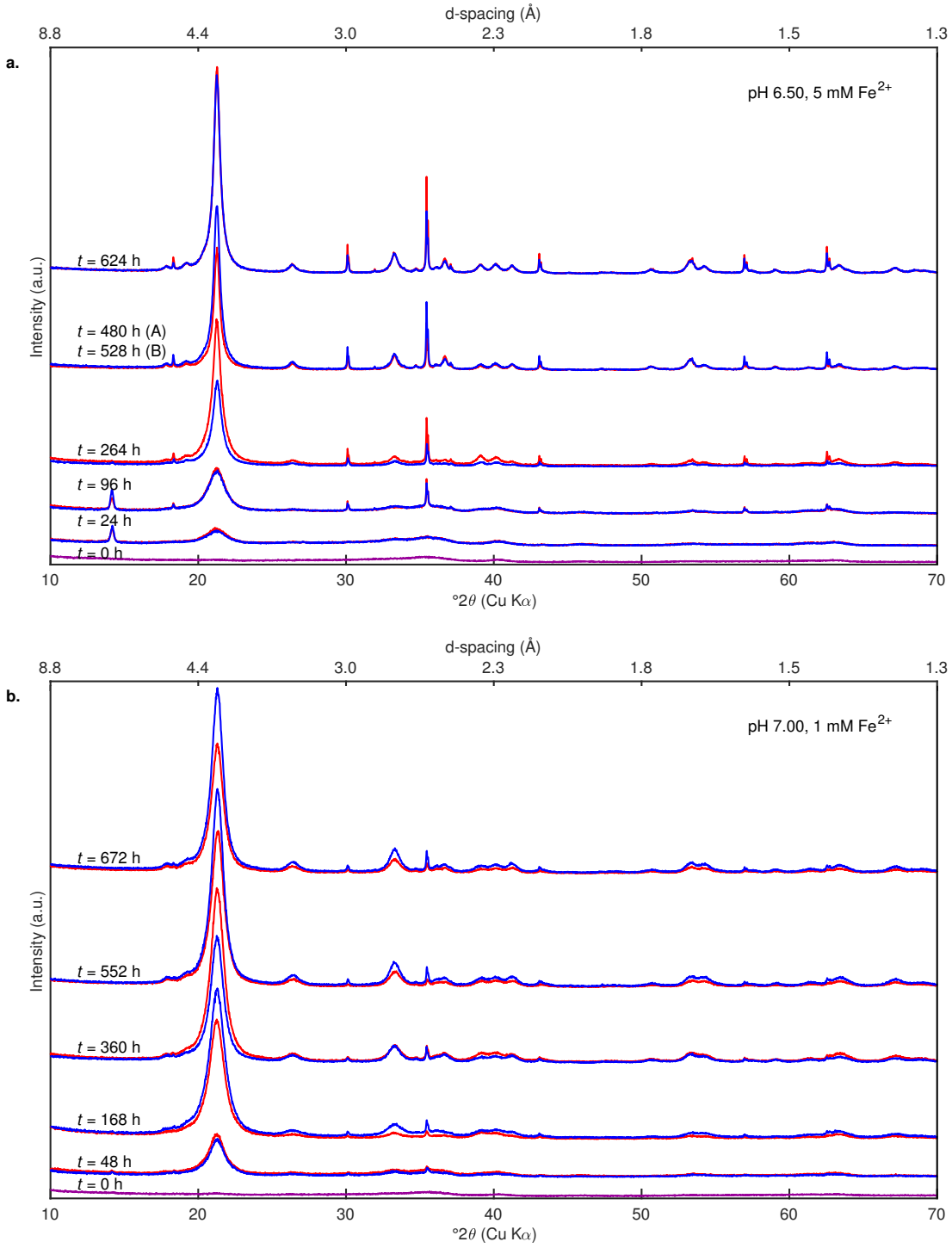

Figure S13 Selected X-ray diffractograms obtained during ferrihydrite transformation experiments at initial Fe^{2+} concentrations of 5 mM at pH 6.50 (**a.**) and at initial Fe^{2+} concentrations of 1 mM at pH 7.00 (**b.**). Sample aliquots were removed from duplicate reactors A (red) and B (blue) at selected time points (t) during the transformations as labelled on the plot.

S8.3 Illustrative example for Rietveld fitting

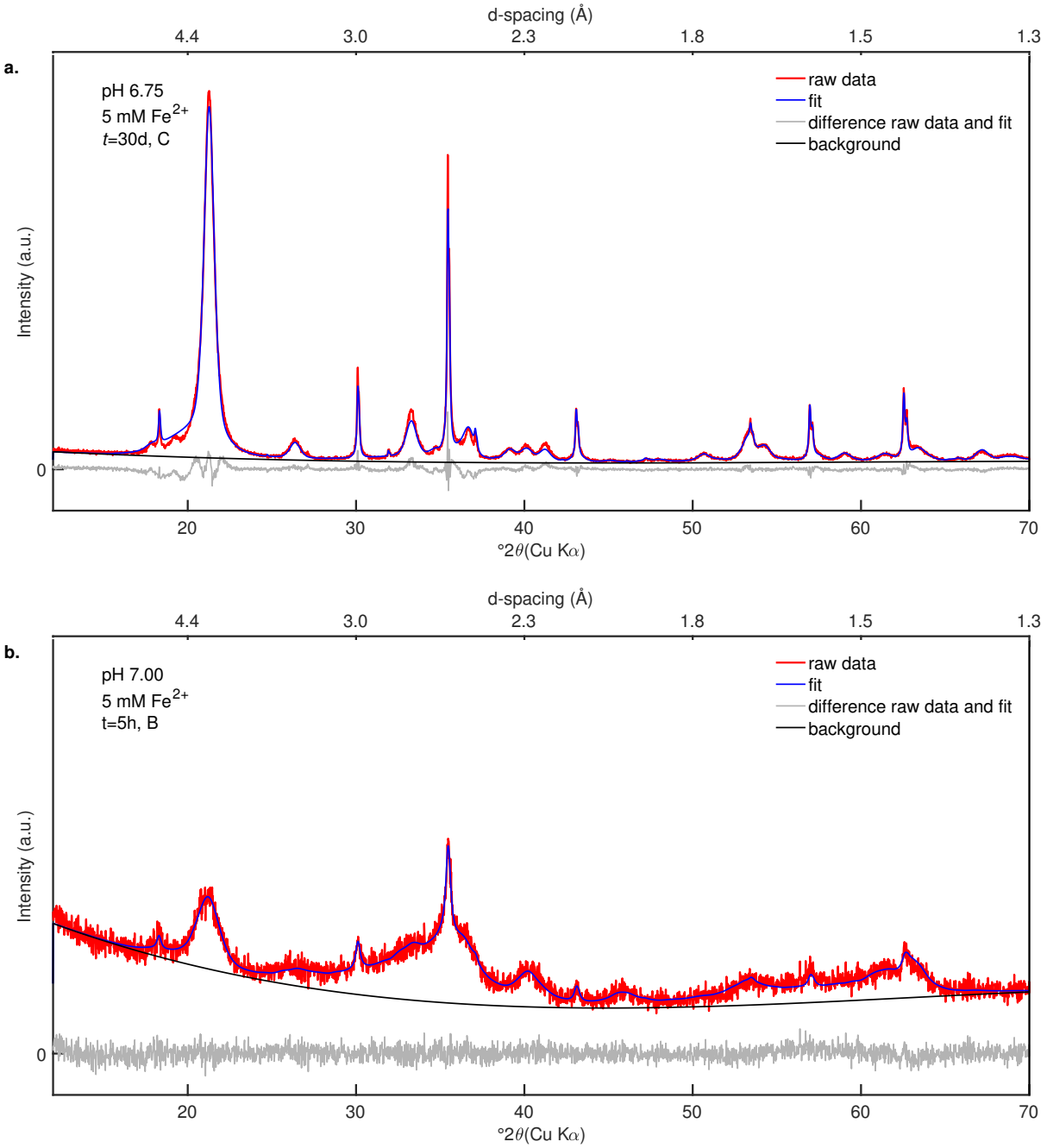

Figure S14 Exemplary fits from Rietveld fitting of X-ray diffractograms. Measured intensities (red), Rietveld fits (blue), the difference between the measured and fitted intensities (light gray) and background intensity (dark grey) are shown. Conditions at which diffractograms were obtained are given on the plot. Exemplary fits are shown for **a.** a sample containing a mixture of goethite and magnetite with traces of siderite (fitted mass fractions of 0.711, 0.285 and 0.004, respectively) and for **b.** a sample containing mainly ferrihydrite (fitted ferrihydrite mass fraction of 0.635 with 0.233 and 0.131 goethite and magnetite, respectively).

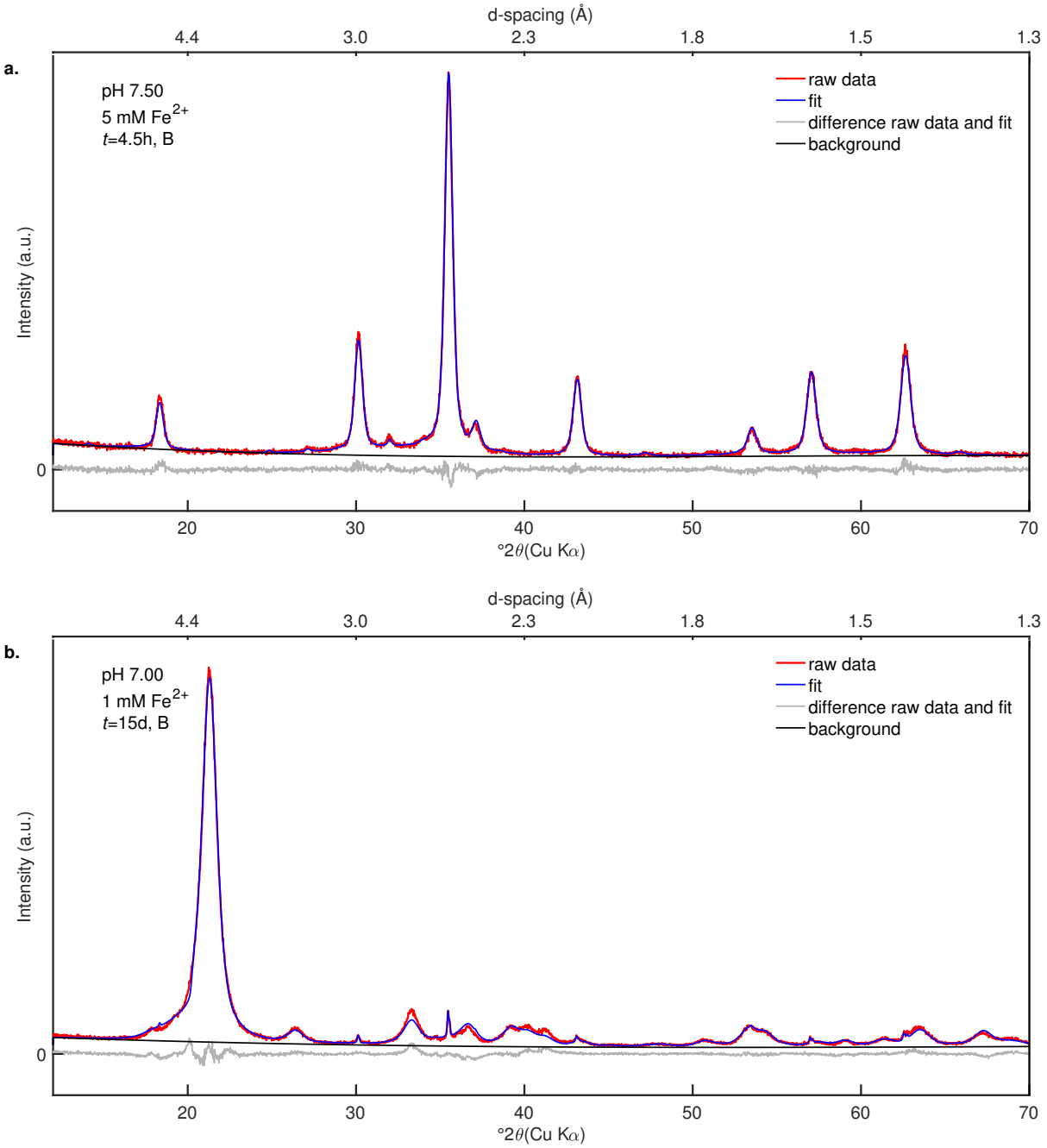

Figure S15 Exemplary fits from Rietveld fitting of X-ray diffractograms. Measured intensities (red), Rietveld fits (blue), the difference between the measured and fitted intensities (light gray) and background intensity (dark grey) are shown. Conditions at which diffractograms were obtained are given on the plot. Exemplary fits are shown for **a.** a sample containing magnetite with traces of siderite and lepidocrocite (fitted mass fractions of 0.98, 0.012 and 0.008, respectively) and for **b.** a sample containing goethite with traces of magnetite and siderite (fitted mass fractions of 0.973, 0.027 and 0.001, respectively).

S8.4 Results of Rietveld fitting

Table S2 Mass fractions of ferrihydrite (hkl phase), magnetite (MAG), goethite (GOE), siderite (SID) and lepidocrocite (LEP) as determined by Rietveld fitting in ferrihydrite transformation experiments at pH 7.50, 7.25 and 7.00 (all at 5 mM initial Fe^{2+}). The goodness of the fit (GOF) corresponds to R_{wp}/R_{exp}, whereby R_{wp} is the weighted profile R factor and R_{exp} is the expected R factor. All fits were of high quality as GOF < 2.

pH	Fe^{2+} (mM)	time (h)	reactor	mass fraction of phase (-)					GOF
				hkl phase	MAG	GOE	SID	LEP	
7.5	5	0.5	A	0.052	0.938	0.000	0.010	0.000	1.276
7.5	5	0.5	B	0.088	0.902	0.000	0.010	0.000	1.128
7.5	5	1.5	A	0.000	0.982	0.000	0.009	0.009	1.474
7.5	5	1.5	B	0.026	0.959	0.000	0.011	0.004	1.294
7.5	5	4.5	A	0.000	0.981	0.000	0.012	0.008	1.242
7.5	5	4.5	B	0.000	0.985	0.000	0.011	0.004	1.225
7.5	5	23	A	0.019	0.963	0.000	0.011	0.007	1.430
7.5	5	23	B	0.025	0.957	0.000	0.011	0.007	1.455
7.25	5	0.5	A	0.221	0.743	0.008	0.024	0.004	1.155
7.25	5	0.5	B	0.136	0.853	0.000	0.009	0.002	1.194
7.25	5	1.5	A	0.170	0.817	0.000	0.011	0.003	1.274
7.25	5	1.5	B	0.228	0.755	0.008	0.009	0.000	1.303
7.25	5	4.5	A	0.137	0.855	0.000	0.008	0.000	1.389
7.25	5	4.5	B	0.133	0.855	0.000	0.012	0.000	1.544
7.25	5	22	A	0.000	0.988	0.000	0.012	0.000	1.343
7.25	5	22	B	0.000	0.985	0.000	0.012	0.003	1.509
7	5	2	A	0.651	0.082	0.265	0.000	0.002	1.089
7	5	2	B	0.646	0.069	0.285	0.000	0.000	1.082
7	5	5	A	0.635	0.131	0.233	0.000	0.000	1.068
7	5	5	B	0.672	0.129	0.199	0.000	0.000	1.067
7	5	8	A	0.592	0.241	0.167	0.000	0.000	1.095
7	5	8	B	0.642	0.124	0.235	0.000	0.000	1.074
7	5	24	A	0.110	0.809	0.072	0.006	0.003	1.161
7	5	24	B	0.324	0.511	0.160	0.005	0.000	1.092
7	5	31	A	0.026	0.809	0.153	0.009	0.003	1.604
7	5	31	B	0.072	0.845	0.071	0.009	0.003	1.446
7	5	53	A	0.027	0.838	0.119	0.011	0.004	1.541
7	5	53	B	0.038	0.811	0.134	0.011	0.006	1.615

Table S3 Mass fractions of ferrihydrite (hkl phase), magnetite (MAG), goethite (GOE), siderite (SID) and lepidocrocite (LEP) as determined by Rietveld fitting in ferrihydrite transformation experiments at pH 6.75, 6.50 (both at 5 mM initial Fe^{2+}), and at 1 mM initial Fe^{2+} (pH 7.00 (5 mM). The goodness of the fit (GOF) corresponds to R_{wp}/R_{exp}, whereby R_{wp} is the weighted profile R factor and R_{exp} is the expected R factor. The fit is considered high quality if GOF < 2. Fits not fulfilling this criterion are marked with $*$.

pH	Fe^{2+} (mM)	time (h)	reactor	mass fraction of phase (-)					GOF
				hkl phase	MAG	GOE	SID	LEP	
6.75	5	192	A	0.266	0.114	0.618	0.001	0.000	1.157
6.75	5	192	B	0.173	0.139	0.686	0.002	0.000	1.308
6.75	5	456	A	0.007	0.249	0.739	0.004	0.000	1.708
6.75	5	456	B	0.012	0.315	0.670	0.004	0.000	1.403
6.75	5	720	A	0.000	0.161	0.837	0.002	0.000	2.320$*$
6.75	5	720	B	0.000	0.285	0.711	0.004	0.000	1.771
6.5	5	24	A	0.607	0.020	0.360	0.000	0.013	1.092
6.5	5	24	B	0.604	0.025	0.351	0.000	0.020	1.096
6.5	5	96	A	0.549	0.083	0.362	0.000	0.006	1.245
6.5	5	96	B	0.534	0.072	0.384	0.001	0.008	1.252
6.5	5	264	A	0.181	0.109	0.708	0.002	0.000	1.586
6.5	5	264	B	0.216	0.104	0.678	0.002	0.000	1.271
6.5	5	480	A	0.000	0.113	0.885	0.002	0.000	1.365
6.5	5	528	B	0.000	0.175	0.822	0.003	0.000	1.551
6.5	5	624	A	0.000	0.158	0.839	0.004	0.000	1.775
6.5	5	624	B	0.000	0.121	0.877	0.002	0.000	1.928
7	1	48	A	0.464	0.031	0.505	0.000	0.000	1.150
7	1	48	B	0.373	0.044	0.583	0.000	0.000	1.189
7	1	168	A	0.110	0.021	0.869	0.000	0.000	1.584
7	1	168	B	0.188	0.028	0.784	0.000	0.000	1.980
7	1	360	A	0.000	0.027	0.973	0.001	0.000	1.995
7	1	360	B	0.000	0.025	0.975	0.000	0.000	1.910
7	1	552	A	0.000	0.013	0.986	0.001	0.000	2.244$*$
7	1	552	B	0.000	0.029	0.970	0.001	0.000	2.653$*$
7	1	672	A	0.000	0.026	0.972	0.002	0.000	1.922
7	1	672	B	0.000	0.037	0.963	0.001	0.000	2.494$*$

S8.5 Calculation of molar ferric iron fractions

The molar fractions of Fe^{III} in ferrihydrite (FH), goethite (GOE) and magnetite (MAG) ($f_{\mathrm{FH/GOE/MAG},t}$) were determined from the mass fractions of these iron oxides obtained from XRD analysis ($mf_{\mathrm{FH/GOE/MAG},t}$) using eqs. S1-S3.

$$f_{\mathrm{FH/GOE/MAG},t} = \frac{\mathrm{n}_{\mathrm{FH/GOE/MAG},t}}{\mathrm{n}_{\mathrm{tot},t}} \tag{S1}$$

where $\mathrm{n}_{\mathrm{FH/GOE/MAG},t}$ are the moles of Fe^{III} in FH, GOE or MAG at time t (calculated using eq. S2), and $\mathrm{n}_{\mathrm{tot},t}$ are the total moles of Fe^{III} at time t (i.e., $\mathrm{n}_{\mathrm{tot}}$ corresponds to the sum of the moles of Fe^{III} in FH, GOE and MAG at time t).

$$\mathrm{n}_{\mathrm{FH/GOE/MAG},t} = \frac{\mathrm{m}_{\mathrm{tot},t} \cdot mf_{\mathrm{FH/GOE/MAG},t}}{\mathrm{M}_{\mathrm{W}}^{\mathrm{FH/GOE/MAG}}} \tag{S2}$$

where $\mathrm{M}_{\mathrm{w,\ FH/GOE/MAG},t}$ are the molar masses of the iron oxides normalized to Fe^{III} (based on their atomic structure, i.e. 107 g $\mathrm{mol}^{-1}_{\mathrm{Fe^{III}}}$ for ferrihydrite ($Fe(OH)_3$), 89 g $\mathrm{mol}^{-1}_{\mathrm{Fe^{III}}}$ for goethite (α-FeOOH), and 116 g $\mathrm{mol}^{-1}_{\mathrm{Fe^{III}}}$ for magnetite ($Fe(III)_2Fe(II)_1O_4$)), and $\mathrm{m}_{\mathrm{tot},t}$ is the total mass of iron oxide present at time t (calculated using eq. S3).

$$\mathrm{m}_{\mathrm{tot},t} = \mathrm{n}_{\mathrm{Fe^{III}},t} \cdot (\mathrm{M}_{\mathrm{W}}^{\mathrm{FH}} \cdot f_{\mathrm{FH},t} + \mathrm{M}_{\mathrm{W}}^{\mathrm{GOE}} \cdot f_{\mathrm{GOE},t} + \mathrm{M}_{\mathrm{W}}^{\mathrm{MAG}} \cdot f_{\mathrm{MAG},t}) \tag{S3}$$

where $\mathrm{n}_{\mathrm{Fe^{III}},t}$ are the moles of Fe^{III} present at time t. Inserting eqs. S2 and S3 into eq. S1 yields eq. S4.

$$f_{\mathrm{FH/GOE/MAG},t} = \frac{(\mathrm{M}_{\mathrm{W}}^{\mathrm{FH}} \cdot f_{\mathrm{FH},t} + \mathrm{M}_{\mathrm{W}}^{\mathrm{GOE}} \cdot f_{\mathrm{GOE},t} + \mathrm{M}_{\mathrm{W}}^{\mathrm{MAG}} \cdot f_{\mathrm{MAG},t}) \cdot mf_{\mathrm{FH/GOE/MAG},t}}{\mathrm{M}_{\mathrm{W}}^{\mathrm{FH/GOE/MAG}}} \tag{S4}$$

S8.6 Magnetite stoichiometry

We determined magnetite stoichiometries from the fitted unit-cell lengths of magnetite according to the following relationship published in Figure 7 in Gorski and Scherer [4].

$$x_d = \frac{a - 8.3424}{0.1094} \tag{S5}$$

where x_d is the stoichiometry of magnetite (i.e. the ratio of Fe^{II}/Fe^{III} in the magnetite structure), and a [Å] is the unit-cell length of magnetite derived from XRD analysis (Section S8.3).

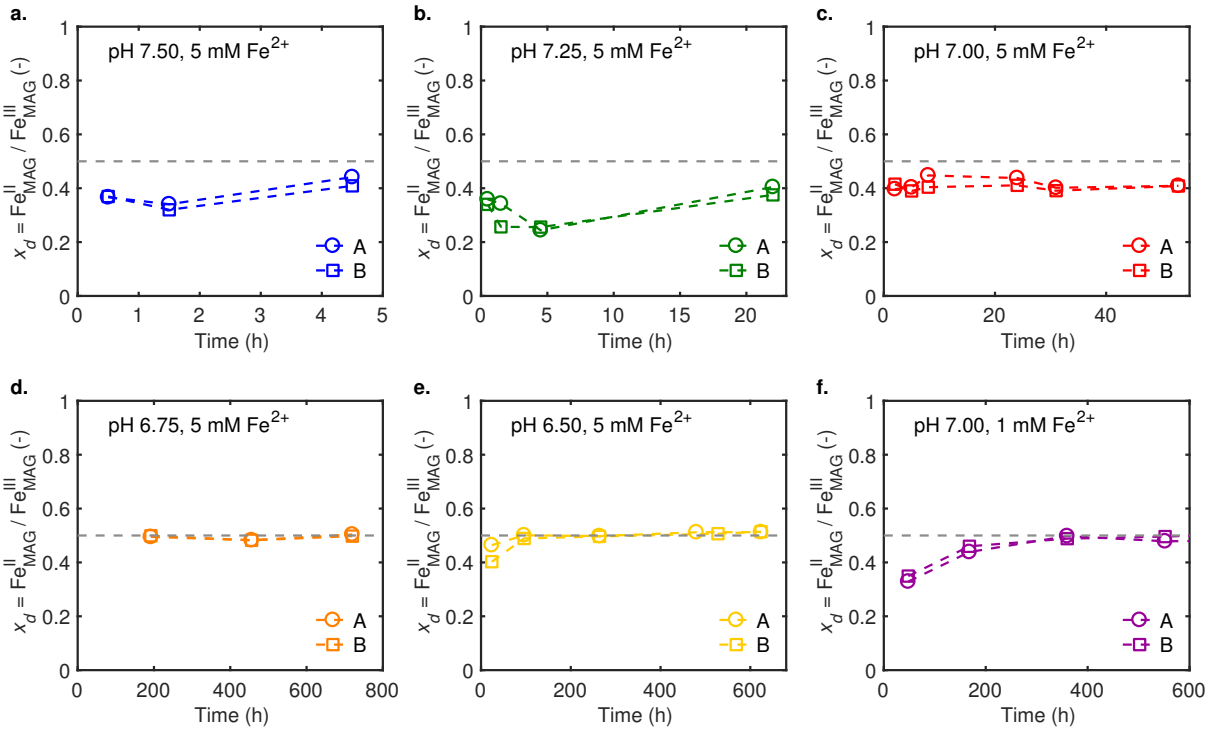

Figure S16 Changes in magnetite stoichiometries, $x_d = Fe^{II}_{MAG}/Fe^{III}_{MAG}$, during ferrihydrite transformation experiments at an initial Fe^{2+} concentration of 5 mM at pH 7.50 (**a.**), pH 7.25 (**b.**), pH 7.00 (**c.**), pH 6.75 (**d.**), pH 6.50 (**e.**) and at an initial Fe^{2+} concentration of 1 mM at pH 7.00 (**f.**). Results are shown for duplicate reactors A (circles) and B (squares). Magnetite stoichiometries were determined using eq. S5.

S8.7 Transformation kinetics

We determined pseudo-first order rate constants for the transformation of ferrihydrite (FH) into goethite (GOE), $k_{\mathrm{FH}\rightarrow\mathrm{GOE}}$ (in units h^{-1}), and into magnetite (MAG), $k_{\mathrm{FH}\rightarrow\mathrm{MAG}}$, by simultaneously fitting eqs. S6-S8 to the changes in calculated molar concentrations (C, in mM $\mathrm{Fe^{III}}$) using Matlab (MathWorks, see Section S8.8 for the Matlab code and Section S8.7 for the fits). Calculated molar concentrations were corrected for dilution of the iron oxide suspension by base addition in pH-stat titration and for the repeated extraction of suspension aliquots for analysis) of these three iron oxides during the transformation experiments We obtained C by multiplying the molar fractions of $\mathrm{Fe^{III}}$ (see above) with the initial concentration of $\mathrm{Fe^{III}}$ (10 mM).

$$\frac{d\mathrm{C_{FH}}(t)}{dt} = -(k_{\mathrm{FH}\rightarrow\mathrm{GOE}} + k_{\mathrm{FH}\rightarrow\mathrm{MAG}}) \cdot \mathrm{C_{FH}}(t) \tag{S6}$$

$$\frac{d\mathrm{C_{GOE}}(t)}{dt} = k_{\mathrm{FH}\rightarrow\mathrm{GOE}} \cdot \mathrm{C_{FH}}(t) \tag{S7}$$

$$\frac{d\mathrm{C_{MAG}}(t)}{dt} = k_{\mathrm{FH}\rightarrow\mathrm{MAG}} \cdot \mathrm{C_{FH}}(t) \tag{S8}$$

We did not fit the kinetics of ferrihydrite transformation into siderite and lepidocrocite because only traces of these minerals formed (mass fractions < 0.02 under all experimental conditions).

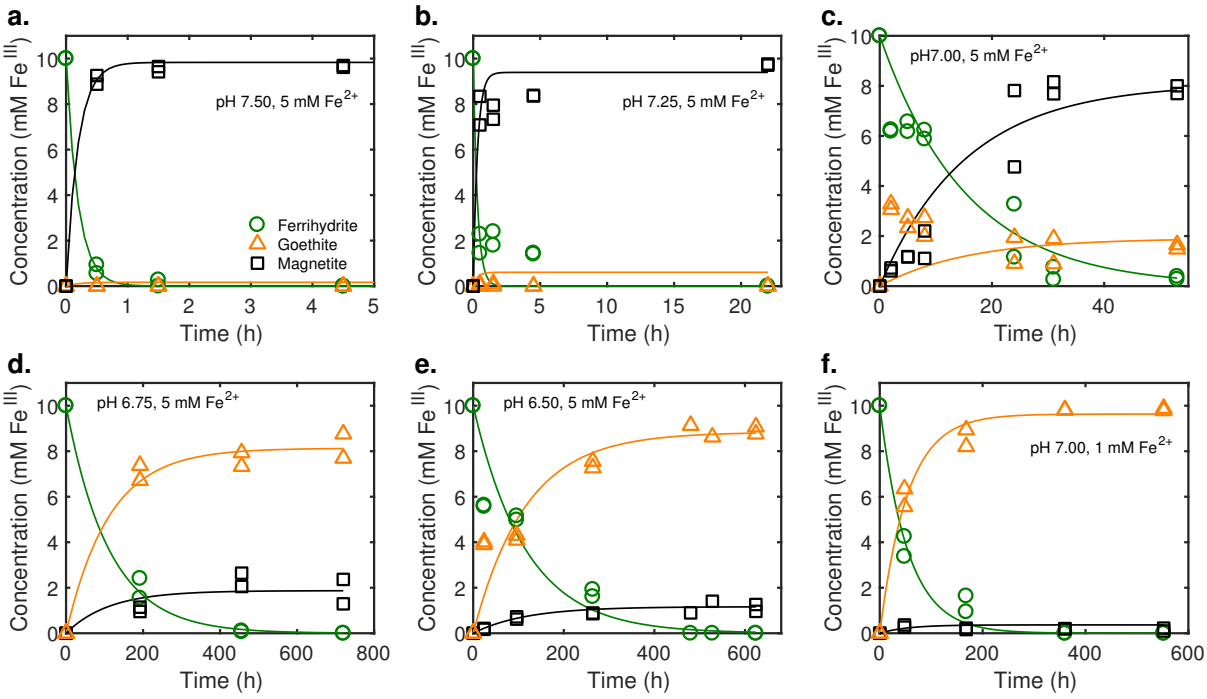

Figure S17 Fitting of ferrihydrite transformation kinetics. Concentrations of $\mathrm{Fe^{III}}$ in the iron oxides were calculated as described in materials and methods. The solid lines represent fitting of a pseudo-first order rate model (eqs. S6 - S8 in the main manuscript) to the data. The fitted rate constants for ferrihydrite transformation into goethite and magnetite are shown in Figure S18.

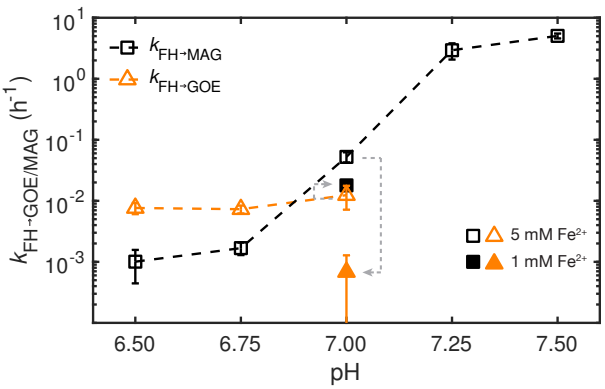

Figure S18 Pseudo-first order rate constants for the transformations of ferrihydrite (FH) into goethite (GOE), $k_{FH\rightarrow GOE}$ and into magnetite (MAG), $k_{FH\rightarrow MAG}$ as a function of the pH of the transformation experiment. Rate constants were determined by fitting eqs. S6–S8 in the main manuscript to the concentrations of Fe^{III} in ferrihydrite, goethite and magnetite (see Figures 1a,b and 3a-d in the main manuscript for molar Fe^{III} fractions in ferrihydrite, goethite and magnetite). Error bars represent the 95% confidence intervals of the kinetic fitting. Dashed grey arrows signify a a decrease in initial Fe^{2+} concentration from 5 to 1 mM.

S8.8 Matlab code for analysis of transformation kinetics

We determined pseudo-first order rate constants for the transformation of ferrihydrite into goethite and magnetite (eqs. S6 to S8 in the main manuscript) using the nlinfit function in Matlab (MathWorks) shown in the code below.

```
%% Import Data
[ExcName,ExcPath]=uigetfile('*.xlsx','Select XRD_PONCKS');
ExStartLine=2;

ExSheet='pH 6.5';
data_xrd_pH65=xlsread([ExcPath,ExcName],ExSheet);
data_xrd_pH65(:,4)=data_xrd_pH65(:,4)/100;
data_xrd_pH65(:,5)=data_xrd_pH65(:,5)/100;
data_xrd_pH65(:,6)=data_xrd_pH65(:,6)/100;
data_xrd_pH65(:,7)=data_xrd_pH65(:,7)/100;
data_xrd_pH65(:,8)=data_xrd_pH65(:,8)/100;

%% pH6.5
pH65_t=[data_xrd_pH65(1:12,2)];
pH65_FH=[data_xrd_pH65(1:12,4)];
pH65_GOE=[data_xrd_pH65(1:12,6)];
pH65_MAG=[data_xrd_pH65(1:12,5)];

% Define fitting functions and parameters, with identical k1 and k2
% for all data sets
mdl1 = @(beta,x) 1*exp(-(beta(1)+beta(2))*x);
mdl2 = @(beta,x) 1*beta(1)/(beta(1)+beta(2)) . . .
-(1*beta(1))/(beta(1)+beta(2))*exp(-(beta(1)+beta(2))*x);
mdl3 = @(beta,x) 1*beta(2)/(beta(1)+beta(2)) . . .
-(1*beta(2))/(beta(1)+beta(2))*exp(-(beta(1)+beta(2))*x);

% Prepare input for NLINMULTIFIT and perform fitting
x_cell = {pH65_t, pH65_t, pH65_t};
y_cell = {pH65_FH, pH65_GOE, pH65_MAG};
mdl_cell = {mdl1, mdl2, mdl3};
beta_pH650 = [0.01, 0.01];
[beta_pH65,r,J,Sigma,mse_pH65,errorparam_pH65,robustw_pH65] = ...
                    nlinmultifit(x_cell, y_cell, mdl_cell, beta_pH650);

% Calculate model predictions and confidence intervals
[ypred1_pH65,Δ1_pH65] = nlpredci(mdl1,pH65_t,beta_pH65,r,'covar',Sigma);
[ypred2_pH65,Δ2_pH65] = nlpredci(mdl2,pH65_t,beta_pH65,r,'covar',Sigma);
[ypred3_pH65,Δ3_pH65] = nlpredci(mdl3,pH65_t,beta_pH65,r,'covar',Sigma);

% Calculate parameter confidence intervals
ci = nlparci(beta_pH65,r,'Jacobian',J);
```

S9 Thermodynamics of iron oxide reduction in MER

Reductive dissolution of ferrihydrite (denoted as $Fe(OH)_3$), goethite (α-FeOOH) and magnetite (Fe_3O_4) are described by the following reaction eqs. S9-S11.

$$Fe(OH)_3 + e^- + 3H^+ \rightleftharpoons Fe^{2+} + 3H_2O \quad \text{(S9)}$$

$$\alpha\text{-FeOOH} + e^- + 3H^+ \rightleftharpoons Fe^{2+} + 2H_2O \quad \text{(S10)}$$

$$0.5Fe_3O_4 + e^- + 4H^+ \rightleftharpoons 1.5Fe^{2+} + 2H_2O \quad \text{(S11)}$$

In mediated electrochemical reduction (MER), we varied the reaction driving force for iron oxide reduction, $\Delta_r G$ (kJ $mol_{e^-\ transferred}^{-1}$), by controlling the pH_{MER} at which the reduction was carried out and the potential applied to the working electrode of the electrochemical cell, E_H^{MER}.

$$\Delta_r G = -nF \cdot (E_H^{oxide} - E_H^{MER}) \quad \text{(S12)}$$

where n is the number of transferred electrons per overall reaction and F is the Faraday constant. We determined $\Delta_r G$ using n=1, i.e. for the transfer of one electron to one oxide-Fe^{III} atom. E_H^{oxide} can be determined using the Nernst equation S13.

$$E_H^{oxide} = E_H^0 - \frac{RT}{n_{e^-}F} \cdot \ln \frac{\{Fe_{aq}^{2+}\}^{m_{Fe^{2+}}}}{10^{-m_{H^+} \cdot pH}} \quad \text{(S13)}$$

where E_H^0 [V] is the standard reduction potential of the iron oxide, R is the gas constant, T (= 298.15 K) is the absolute temperature at which MER experiments were conducted, $\{Fe_{aq}^{2+}\}$ [mol L^{-1}] is the activity of aqueous Fe^{2+}, and $m_{Fe^{2+}}$, m_{H^+} and n_{e^-} denote the stoichiometric coefficients for Fe^{2+}, H^+ and e^- in eqs. S9 to S11.

In Figure S19, E_H-pH stability diagrams for ferrihydrite, goethite and magnetite are plotted. The diagrams were created using an activity coefficient for Fe^{2+} of 0.785[10], Fe^{2+} concentrations corresponding to the addition of 20 μL iron oxide suspension containing 1 and 5 mM Fe^{2+} to the electrochemical cells, and E_H^0 values of 0.98 V[11] for ferrihydrite and 0.768 V[12] for goethite. For magnetite, we used E_H^0 = 0.98 V[13]. However, this values is strongly dependent on magnetite stoichiometry[14] and particle size[13] and thus the E_H-pH stability area in Figure S19c for magnetite may not accurately describe the stability of the magnetite formed in the transformation experiments herein.

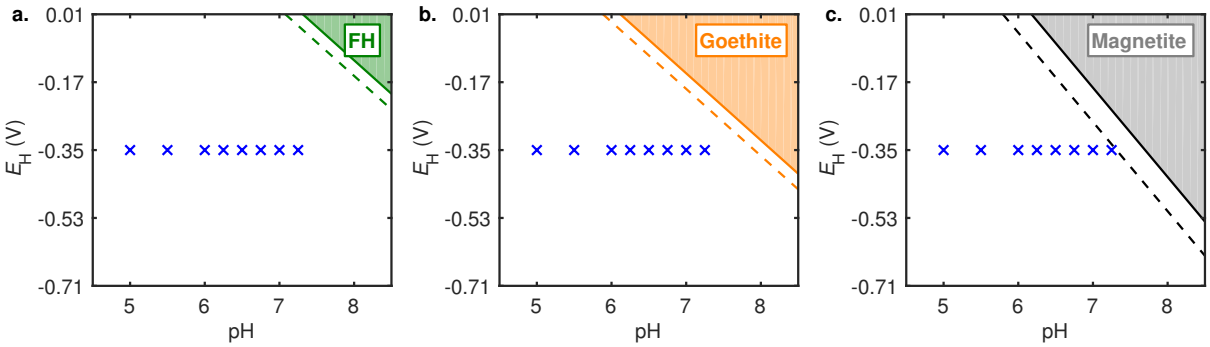

Figure S19 E_H-pH stability diagrams of ferrihydrite (FH, **a.**), goethite (**b.**) and magnetite (**c.**). Diagrams were created using standard reduction potentials (E^0_H) of 0.98 V[11] for ferrihydrite, E^0_H = 0.768 V for goethite[12] and E^0_H = 0.98 V for magnetite[13]. The E_H-pH stability diagrams were created using Fe^{2+} concentrations of 3.64 μM (this concentration corresponds to the concentration in the electrochemical cell after addition of 20 μL sample suspension containing 1 mM Fe^{2+}, solid lines) and 18.1 μM (corresponding to the concentration in the electrochemical cell after addition of 20 μL sample suspension containing 5 mM Fe^{2+}, dashed lines). The blue crosses depict the E_H-pH conditions in mediated electrochemical reduction measurements. We deliberately chose these E_H-pH conditions to result in exergonic free energies of iron oxide reductive dissolution for all three studied iron oxides (with the only exception of magnetite reduction at pH_{MER} = 7.25, at which the reduction potential applied to the electrochemical cell approximately equaled the estimated reduction potential of magnetite ferric iron in the presence of 18.1 μM Fe^{2+}).

S10 Experimental current response during MER measurement

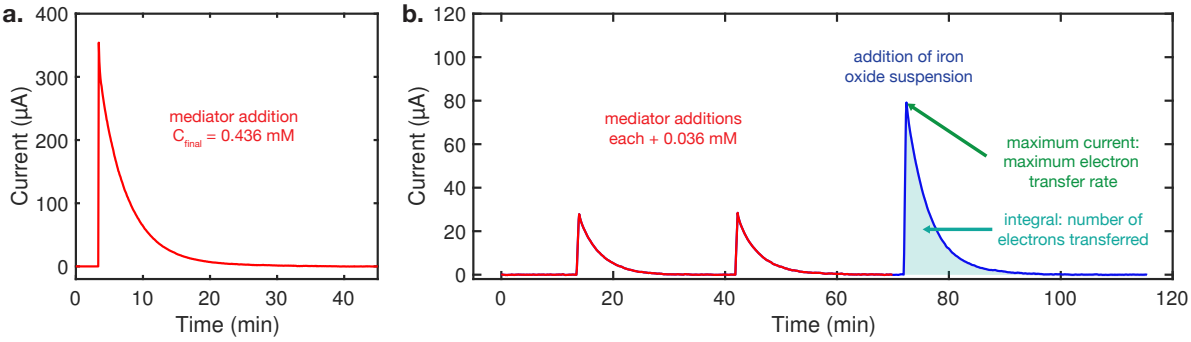

Figure S20 Addition scheme of mediator and iron oxide in a mediated electrochemical reduction experiment of hematite at pH 5.00, $E_{\mathrm{H}}^{\mathrm{MER}} = -0.35$ V. **a.** The first large addition of mediator resulted in a final concentration of electron transfer mediator diquat in the electrochemical cell of 0.436 mM. **b.** The smaller second and third diquat additions (red) each resulted in an increase of mediator concentration in the electrochemical cell by 0.036 mM. These smaller mediator additions were followed by addition of iron oxide suspension (blue). The number of electrons transferred and the maximum electron transfer during each reductive current peak were determined from the peak integral and the maximum peak current, respectively.

S11 Matlab code for the analysis of MER measurements

Analysis of peaks in reductive current responses was performed using the baseline fit function and the bioinformatics toolbox in Matlab as shown below.

```
% ------------------------------------------------------------------------
% import data
% ------------------------------------------------------------------------
[FName,PathName]=uigetfile('*.txt','Select Text file');
sample=importdata([PathName,FName]);
% number of measurement _xxx
time_xxx=sample.data(:,1);

for i=2:length(time_xxx);
    if time_xxx(i)-time_xxx(i-1)==10;
        time_xxx(i)=time_xxx(i)-5;
    else
        time_xxx(i)=time_xxx(i);
    end
end

Dat_xxx=sample.data(:,2:9);
% ------------------------------------------------------------------------
% baseline subtraction
% ------------------------------------------------------------------------
[Dat_xxx(:,1),bs(:,1)] = bf(Dat_xxx(:,1),'confirm',16);
[Dat_xxx(:,2),bs(:,2)] = bf(Dat_xxx(:,2),'confirm',16);
[Dat_xxx(:,3),bs(:,3)] = bf(Dat_xxx(:,3),'confirm',16);
[Dat_xxx(:,4),bs(:,4)] = bf(Dat_xxx(:,4),'confirm',16);
[Dat_xxx(:,5),bs(:,5)] = bf(Dat_xxx(:,5),'confirm',16);
[Dat_xxx(:,6),bs(:,6)] = bf(Dat_xxx(:,6),'confirm',16);
[Dat_xxx(:,7),bs(:,7)] = bf(Dat_xxx(:,7),'confirm',16);
[Dat_xxx(:,8),bs(:,8)] = bf(Dat_xxx(:,8),'confirm',16);
% ------------------------------------------------------------------------
% save baseline subtraction
% ------------------------------------------------------------------------
csvwrite('bs_xxx.csv',Dat_xxx)
% ------------------------------------------------------------------------
% manually select start and end points of peaks and save
% as c1, c2 etc.
% ------------------------------------------------------------------------
msviewer(time_xxx,Dat_xxx(:,1))
% ------------------------------------------------------------------------
% User Input Section
% ------------------------------------------------------------------------
NPeaks=[3,3,3,3,3,3,3,3]; % _xxx
sep=[c1,c2,c3,c4,c5,c6,c7,c8];
sep_start=sep([1:2:5],:); % select all peak start points
sep_start=round(sep_start./5)*5/5; % round to 5 (as dt=5)
```

```
sep_end=sep([2:2:6],:); % select all peak end points
sep_end=round(sep_end./5)*5/5; % round to 5 (as dt=5)
% ------------------------------------------------------------------------
% Parameters and matrices
% ------------------------------------------------------------------------
f=96485.3365;
dt=5;
Out=zeros(sum(NPeaks),2);
% ------------------------------------------------------------------------
% Loop over currents and peaks
% ------------------------------------------------------------------------
for i=1:length(Dat_xxx(1,:)) % for currents 1 to 8

    for j=1:NPeaks(i) % for all peaks
        i1=sep_start(j,i);
        i2=sep_end(j,i);
        sI=Dat_xxx(i1:i2,i);

        % Peak maximum
        clear ind_imax
        [¬,ind_imax]=max(sI);
        clear imax
        imax=max(sI);
        Out(sum(NPeaks(1:(i-1)))+j,1)=imax;

        % Integration
        clear int
        int=zeros(1,length(sI));
        int(1)=0;
        for k=2:length(sI)
            int(k)=int(k-1)+((sI(k)+sI(k-1))/2)*dt;
        end
        int=int/f;
        Out(sum(NPeaks(1:(i-1)))+j,2)=int(end);
% ------------------------------------------------------------------------
% Prepare Output
% ------------------------------------------------------------------------
        RawDatOut_xxx(sum(NPeaks(1:(i-1)))+j,1:i2-i1+1)=[sI];
    end
end
% ------------------------------------------------------------------------
% Write Output
% ------------------------------------------------------------------------
RawDatOut_xxx(sum(NPeaks(1:(i-1)))+j+1,1:length(time_xxx))=[time_xxx];
csvwrite('Output_xxx.csv',Out)
```

S12 Proton release during ferrihydrite transformations

S12.1 Reaction equations for ferrihydrite transformations

Reaction equations for ferrihydrite (denoted as 'Fe(OH)$_3$' in eqs. S14 and S15) transformation into goethite (α-FeOOH, eq. S14) and magnetite (shown for stoichiometric magnetite $Fe^{III}{}_2Fe^{II}{}_1O_4$ in eq. S15).

$$\text{'Fe(OH)}_3\text{'} + Fe^{2+} \longrightarrow \alpha\text{-FeOOH} + H_2O + Fe^{2+} \tag{S14}$$

$$\text{'Fe(OH)}_3\text{'} + Fe^{2+} \longrightarrow 0.5\ Fe^{III}_2Fe^{II}O_4 + H_2O + H^+ + 0.5\ Fe^{2+} \tag{S15}$$

The stoichiometry of ferrihydrite transformation into goethite does not involve net uptake or release of H^+ and Fe^{2+} (eq. S14). Conversely, magnetite formation involves H^+ release into solution (one mole of H+ per mole of FeIII) and Fe^{2+} incorporation into the magnetite structure (eq. S15). For ease of reaction balancing, we use the most simplistic representation of ferrihydrite stoichiometry in eqs. S14 and S15. We note, however, that the release of H^+ relative to oxide Fe^{III} during ferrihydrite transformation into goethite (H^+/Fe^{III}=0) or magnetite (H^+/Fe^{III}=1) remains unchanged irrespective of the stoichiometry chosen for ferrihydrite.

S12.2 Calculation of $H^+_{tit}/Fe^{III}_{oxide}$

We determined the ratio of $H^+_{tit}/Fe^{III}_{oxide}$ during ferrihydrite transformation from the moles of H^+ released (n_{H^+}) and the moles of Fe^{III} present ($n_{Fe^{III}}$) at each time point i according to eqs. S16-S17.

$$n_{H^+}(i) = n_{H^+}(i-1) - n_{H^+,\,removed}(i) + (V_{base}(i) - V_{base}(i-1)) \cdot C_{base} \tag{S16}$$

$$n_{Fe^{III}}(i) = n_{Fe^{III}}(i-1) - n_{Fe^{III},\,removed}(i) \tag{S17}$$

where V_{base} is the cumulative volume of titrated base, C_{base} is the concentration of the titrated base (70 mM) and $n_{H^+,\,removed}(i)$ and $n_{Fe^{III},\,removed}(i)$ are the moles of H^+ and Fe^{III} removed at time point i.

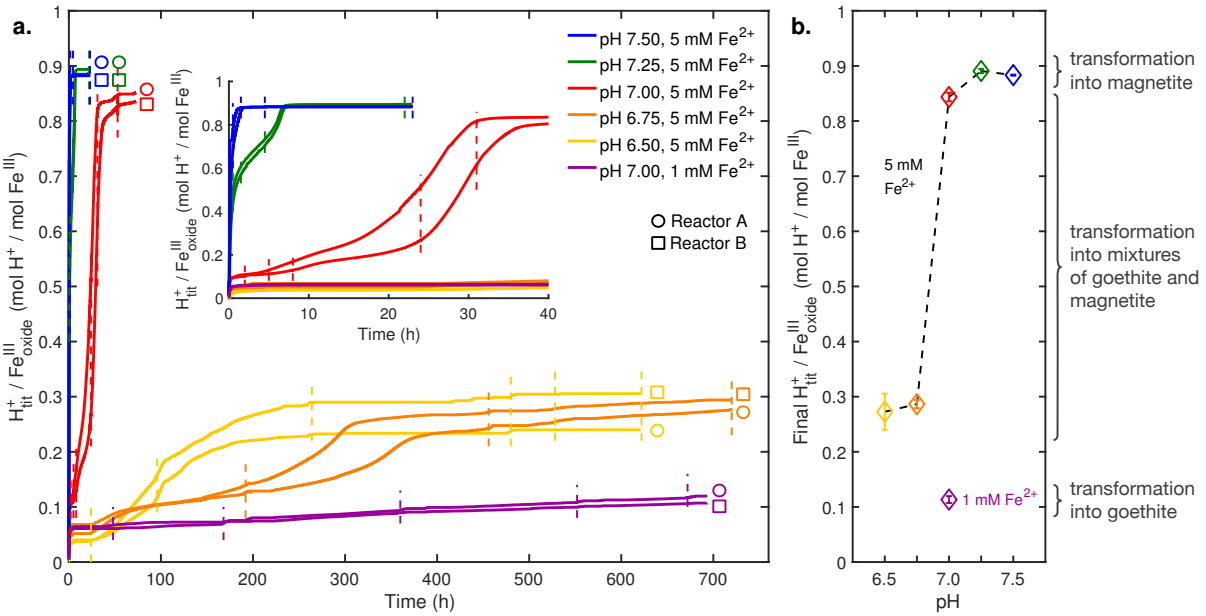

Figure S21 a. The moles of H^+ released per mole of oxide Fe^{III} ($H^+_{tit}/Fe^{III}_{oxide}$, (mol H^+ / mol Fe^{III})) during ferrihydrite transformation experiments. Results are shown for duplicate reactors A (circles) and B (squares). We determined $H^+_{tit}/Fe^{III}_{oxide}$ from the volume and concentration of titrated base and the calculated Fe^{III} concentration remaining in the reactor at each time point during the transformation as described in the text. Vertical dashed lines mark the time points of sample aliquot collection from the reactors for X-ray diffraction, microscopic and electrochemical analyses. The inset shows an enlarged view of H^+ release between 0 and 40 h. **b.** Final $H^+_{tit}/Fe^{III}_{oxide}$ plotted versus the pH of the transformation experiment. The dashed black line connects data from transformation experiments conducted at the same initial Fe^{2+} concentration of 5 mM and is drawn as a guide to the eye. The dashed grey arrow signifies a decrease in initial Fe^{2+} concentration of 5 to 1 mM. The color coding is the same as in a.

S12.3 Modeled H^+ release during ferrihydrite transformation

We modeled the release of H^+ per remaining Fe^{III} ($H^+_{tit}/Fe^{III}_{oxide}\ {}^{calc}_{t}$, in mole H^+ per mole Fe^{III}) using eq. S18.

$$H^+_{tit}/Fe^{III}_{oxide}\ {}^{calc}_{t} = (H^+_{tit}/Fe^{III}_{oxide})\ {}^{MAG}_{t} + (H^+_{tit}/Fe^{III}_{oxide})\ {}^{surf}_{t} \tag{S18}$$

where $(H^+_{tit}/Fe^{III}_{oxide})\ {}^{MAG}_{t}$ is the release of H^+ due to magnetite formation until time t, and $(H^+_{tit}/Fe^{III}_{oxide})\ {}^{surf}_{t}$ is the release of iron oxide-associated H^+ due to Fe^{2+} adsorption to the iron oxide surfaces and decreasing specific iron oxide surface areas until time t. We list calculated values of $H^+_{tit}/Fe^{III}_{oxide}\ {}^{calc}_{t}$, $(H^+_{tit}/Fe^{III}_{oxide})\ {}^{MAG}_{t}$ and $(H^+_{tit}/Fe^{III}_{oxide})\ {}^{surf}_{t}$ in Tables S4 and S5.

We calculated $(H^+_{tit}/Fe^{III}_{oxide})\ {}^{MAG}_{t}$ according to eq. S19.

$$(H^+_{tit}/Fe^{III}_{oxide})\ {}^{MAG}_{t} = nf_{MAG,t} \cdot MAG_{stoich,t} \cdot 2 \tag{S19}$$

where $nf_{MAG,t}$ is the molar fraction of magnetite Fe^{III} at time t (Section S8.5) and $MAG_{stoich,t}$ is the stoichiometry of the magnetite at time t (see Section S8.6). The multiplication factor 2

signifies a release of one mole H^+ per 0.5 mole of Fe^{2+} during the transformation of ferrihydrite into magnetite (eq. S15 in the main manuscript).

We calculated $(H^+_{tit}/Fe^{III}_{oxide})\ ^{surf}_{t}$ according to eq. S20 using results from surface chemistry simulations performed in PHREEQC 3[5] (see Section S12.4 for the employed code).

$$H^+_{tit}/Fe^{III}_{oxide}\ ^{surf}_{t} = \frac{[H^+ \text{ assoc } FH_{ini}] - [H^+ \text{ assoc oxide }_t]}{n_{Fe^{III},t}} \quad \text{(S20)}$$

where $[H^+ \text{ assoc } FH_{ini}]$ are the moles of H^+ associated with the initial ferrihydrite surface prior to addition of Fe^{2+}, and $[H^+ \text{ assoc oxide }_t]$ are the moles of H^+ associated with the iron oxide surfaces at time t. We determined $[H^+ \text{ ads } FH_{ini}]$ from the sum of ferrihydrite surface sites occupied by H^+, i.e. the sum of $2{\cdot}Hfo\_sOH^{2+}$, $2{\cdot}Hfo\_wOH^{2+}$, Hfo_sOH and Hfo_wOH surface sites. To this end, we used the mass of ferrihydrite at $t = 0$ h (calculated from the molar mass of $Fe(OH)_3$ and an Fe^{III} concentration of 10 mM) and a specific surface area (SSA) of ferrihydrite of 213 $m^2\ g^{-1}$ (Table S1) as input parameters in PHREEQC. We determined $[H^+ \text{ assoc oxide }_t]$ from the sum of H^+ associated with ferrihydrite, goethite and magnetite surfaces at time t. In order to simulate H^+ association with the surfaces of ferrihydrite, goethite and magnetite in PHREEQC, we required input parameters for i) SSAs, ii) aqueous Fe^{2+} concentrations, and ii) masses of these oxides.

i) As SSA input parameters, we used 213 $m^2\ g^{-1}$ for ferrihydrite (average of 206.2 and 220.6 $m^2\ g^{-1}$ determined for the two batches of ferrihydrite synthesized according to the same procedure as the ferrihydrite used in the transformation experiments), 17.5 $m^2\ g^{-1}$ for goethite (average of 16.7 and 18.2 $m^2\ g^{-1}$ that we measured for the goethite formed in transformation experiments run at pH 7.00) and 36.4 $m^2\ g^{-1}$ for magnetite (average of 41.7, 41.1, 43.5 and 19.3 $m^2\ g^{-1}$ that we measured for the magnetite formed in transformation experiments run at pH 7.25 and 7.50) (Table S1). We therefore estimated the SSA of iron oxide mixtures at intermittent time points during ferrihydrite transformations from the SSA of the pure transformation products by linearly combining the SSAs of ferrihydrite, goethite and magnetite weighted according to their respective mass fractions. This estimation was necessary because we could not measure iron oxide SSAs at intermittent time points during ferrihydrite transformations as relatively large sample masses are required for N_2-BET analysis.

ii) To obtain the input values for aqueous Fe^{2+} concentrations, we subtracted the Fe^{2+} concentration bound in the magnetite structure at time t from the concentration of Fe^{2+} initially added to the reactors. The concentration of Fe^{2+} bound in the magnetite structure at time t equalled $2{\cdot}C_{MAG,t}{\cdot}MAG_{stoich}$ ($C_{MAG,t}$ was determined from $n_{MAG,t}$ and the suspension volume in the reactor at time t.

iii) We determined the masses of ferrihydrite (FH), goethite (GOE) and magnetite (MAG) at time t ($m_{FH/GOE/MAG,t}$) using eq. S21.

$$m_{FH/GOE/MAG\,t} = f_{FH/GOE/MAG,\ t} \cdot m_{tot,\ t} \quad \text{(S21)}$$

where $f_{FH/GOE/MAG,t}$ are the mass fractions of ferrihydrite, goethite and magnetite at time t

as determined using XRD, and $m_{tot,t}$ is the total iron oxide mass at time t as determined using eq. S22.

$$m_{tot,t} = n_{Fe^{III},t} \cdot (M_W^{FH} \cdot f_{FH,t} + M_W^{GOE} \cdot f_{GOE,t} + \frac{M_W^{MAG}}{2} \cdot f_{MAG,t}) \quad \text{(S22)}$$

where M_W^x is the mass of the iron oxide per mole Fe^{III} (x = FH, GOE, MAG, i.e., 107 g mol^{-1} Fe^{III} for ferrihydrite ($Fe(OH)_3$), 89 g mol^{-1} Fe^{III} for goethite (α-FeOOH), 116 g mol^{-1} Fe^{III} for magnetite ($Fe(III)_2Fe(II)_1O_4$).

Table S4 Modeled release of H^+ per remaining Fe^{III} ($H^+_{tit}/Fe^{III}_{oxide}\ {}^{calc}_{t}$) during ferrihydrite transformation experiments at pH 7.00, 7.25 and 7.50 (all at 5 mM initial Fe^{2+}) due to magnetite formation ($(H^+_{tit}/Fe^{III}_{oxide})\ {}^{MAG}_{t}$) and due to the release of iron oxide-associated H^+ as a consequence of Fe^{2+} adsorption to the iron oxide surfaces and a decrease in specific iron oxide surface area ($(H^+_{tit}/Fe^{III}_{oxide})\ {}^{surf}_{t}$). See text for details on the modeling procedure.

pH	Fe^{2+} (mM)	time (h)	reactor	$(H^+_{tit}/Fe^{III}_{oxide})\ {}^{MAG}_{t}$	$(H^+_{tit}/Fe^{III}_{oxide})\ {}^{surf}_{t}$	$H^+_{tit}/Fe^{III}_{oxide}\ {}^{calc}_{t}$
7.5	5	0	A	0.000	0.000	0.000
7.5	5	0.5	A	0.678	0.094	0.772
7.5	5	1.5	A	0.657	0.095	0.752
7.5	5	4.5	A	0.849	0.097	0.946
7.5	5	23	A	0.699	0.097	0.796
7.5	5	0	B	0.000	0.000	0.000
7.5	5	0.5	B	0.656	0.093	0.749
7.5	5	1.5	B	0.603	0.095	0.697
7.5	5	4.5	B	0.793	0.097	0.890
7.5	5	23	B	0.588	0.097	0.685
7.25	5	0	A	0.000	0.071	0.071
7.25	5	0.5	A	0.508	0.093	0.601
7.25	5	1.5	A	0.545	0.094	0.639
7.25	5	4.5	A	0.409	0.095	0.504
7.25	5	22	A	0.790	0.097	0.887
7.25	5	0	B	0.000	0.071	0.071
7.25	5	0.5	B	0.567	0.092	0.659
7.25	5	1.5	B	0.376	0.093	0.470
7.25	5	4.5	B	0.427	0.095	0.522
7.25	5	22	B	0.729	0.097	0.826
7	5	0	A	0.000	0.056	0.056
7	5	2	A	0.058	0.086	0.144
7	5	5	A	0.095	0.087	0.182
7	5	8	A	0.197	0.088	0.285
7	5	24	A	0.684	0.092	0.776
7	5	31	A	0.617	0.095	0.712
7	5	53	A	0.655	0.095	0.750
7	5	0	B	0.000	0.057	0.057
7	5	2	B	0.051	0.086	0.137
7	5	5	B	0.091	0.087	0.178
7	5	8	B	0.089	0.087	0.176
7	5	24	B	0.391	0.089	0.480
7	5	31	B	0.638	0.093	0.731
7	5	53	B	0.628	0.095	0.723

Table S5 Modeled release of H^+ per remaining Fe^{III} ($H^+_{tit}/Fe^{III}_{oxide}\ {}^{calc}_{t}$) during ferrihydrite transformation experiments at pH 6.50 and 6.75 (both at 5 mM initial Fe^{2+}) and at 1 mM initial Fe^{2+} (pH 7.00) due to magnetite formation ($(H^+_{tit}/Fe^{III}_{oxide})\ {}^{MAG}_{t}$) and due to the release of iron oxide-associated H^+ as a consequence of Fe^{2+} adsorption to the iron oxide surfaces and a decrease in specific iron oxide surface area ($(H^+_{tit}/Fe^{III}_{oxide})\ {}^{surf}_{t}$). See text for details on the modeling procedure.

pH	Fe^{2+} (mM)	time (h)	reactor	$(H^+_{tit}/Fe^{III}_{oxide})\ {}^{MAG}_{t}$	$(H^+_{tit}/Fe^{III}_{oxide})\ {}^{surf}_{t}$	$H^+_{tit}/Fe^{III}_{oxide}\ {}^{calc}_{t}$
6.75	5	0	A	0.000	0.041	0.041
6.75	5	192	A	0.094	0.095	0.189
6.75	5	456	A	0.198	0.096	0.294
6.75	5	720	A	0.130	0.098	0.228
6.75	5	0	B	0.000	0.040	0.040
6.75	5	192	B	0.114	0.094	0.208
6.75	5	456	B	0.255	0.096	0.350
6.75	5	720	B	0.235	0.098	0.333
6.5	5	0	A	0.000	0.023	0.023
6.5	5	24	A	0.016	0.095	0.111
6.5	5	96	A	0.072	0.097	0.169
6.5	5	264	A	0.089	0.099	0.187
6.5	5	480	A	0.092	0.099	0.190
6.5	5	624	A	0.129	0.099	0.228
6.5	5	0	B	0.000	0.023	0.023
6.5	5	24	B	0.017	0.095	0.112
6.5	5	96	B	0.061	0.096	0.157
6.5	5	264	B	0.085	0.098	0.184
6.5	5	528	B	0.142	0.098	0.241
6.5	5	624	B	0.099	0.098	0.197
7	1	0	A	0.000	0.033	0.033
7	1	48	A	0.017	0.087	0.104
7	1	168	A	0.014	0.087	0.102
7	1	360	A	0.020	0.088	0.108
7	1	552	A	0.010	0.092	0.102
7	1	672	A	0.019	0.096	0.115
7	1	0	B	0.000	0.033	0.033
7	1	48	B	0.025	0.056	0.082
7	1	168	B	0.021	0.087	0.108
7	1	360	B	0.019	0.087	0.106
7	1	552	B	0.022	0.089	0.111
7	1	672	B	0.029	0.093	0.122

S12.4 PHREEQC code

We modelled the association of H^+ with iron oxides surfaces using the chemical speciation software PHREEQC 3[5]. As input parameters, we used surface site densities for H^+ association and Fe^{2+} adsorption of 2.27 nm^{-2} for ferrihydrite[6], 1.68 nm^{-2} for goethite[6] and 2.05 nm^{-2} for magnetite[7]. H^+ and Fe^{2+} adsorption constants for strong and weak binding sites on ferrihydrite (hfo) were from Appelo et al.[8] and Liger et al.[6], respectively, adsorption constants for goethite from Liger et al.[6] and Dixit and Hering[9] and adsorption constants for magnetite from Liger et al.[6].

```
SURFACE_MASTER_SPECIES
  Surfmag SurfmagOH
  Surfgoe SurfgoeOH

SURFACE_SPECIES
        Hfo_sOH  + H+ = Hfo_sOH2+
        log_k  7.18

        Hfo_sOH = Hfo_sO- + H+
        log_k  -8.82

        Hfo_sOH + Fe+2 = Hfo_sOFe+ + H+
        log_k  -0.95

        Hfo_wOH  + H+ = Hfo_wOH2+
        log_k  7.18

        Hfo_wOH = Hfo_wO- + H+
        log_k  -8.82

        Hfo_wOH + Fe+2 = Hfo_wOFe+ + H+
        log_k  -2.98

        Hfo_wOH + Fe+2 + H2O = Hfo_wOFeOH + 2H+
        log_k  -11.55

  SurfgoeOH = SurfgoeOH
  log_k     0
  SurfgoeOH + H+ = SurfgoeOH2+
  log_k     7.47
  SurfgoeOH = SurfgoeO- + H+
  log_k     -9.51
  SurfgoeOH + Fe+2 = SurfgoeOFe+ + H+
  log_k     -0.54
  SurfgoeOH + Fe+2 + H2O = SurfgoeOFeOH + 2H+
  log_k     -7.64

  SurfmagOH = SurfmagOH
```

```
  log_k     0
  SurfmagOH + H+ = SurfmagOH2+
  log_k     6.26
  SurfmagOH = SurfmagO- + H+
  log_k     -7.32
  SurfmagOH + Fe+2 = SurfmagOFe+ + H+
  log_k     -1.05
  SurfmagOH + Fe+2 + H2O = SurfmagOFeOH + 2H+
  log_k     -9

PHASES
       Fix_H+
     H+ = H+
     log_k 0
SOLUTION 2
   pH        6.5
   units     mol/kgw
   Cl        1e-3
END

SELECTED_OUTPUT
-file exp_pH65_Fe50.txt
-molalities    Fe+3 Fe+2 Hfo_sOH2+ Hfo_sO- Hfo_wOH2+ Hfo_wO- Hfo_sOFe+ ...
    Hfo_wOFe+ Hfo_wOFeOH Hfo_sOH Hfo_wOH SurfgoeOH SurfgoeOH2+ SurfgoeO- ...
    SurfgoeOFe+ SurfgoeOFeOH SurfmagOH SurfmagOH2+ SurfmagO- SurfmagOFe+ ...
    SurfmagOFeOH
-totals Fe
#---------------------------------------------------------------------
# t-1 A
USE solution 2
SURFACE 1
        Hfo_sOH        2.09e-5    213.    1.064
        Hfo_wOH        8.34e-4

EQUILIBRIUM_PHASES 1
   Fix_H+ -6.5 HCl
END
#---------------------------------------------------------------------
# t0 A
SOLUTION 1
   pH        6.5
   units     mol/kgw
   Fe(2)     5e-3
   Cl        10e-3
SURFACE 1
        Hfo_sOH        2.09e-5    213.    1.065
        Hfo_wOH        8.34e-4

EQUILIBRIUM_PHASES 1
   Fix_H+ -6.5 HCl
```

```
END
#----------------------------------------------------------------
# t1 A
SOLUTION 1
   pH        6.5
   units     mol/kgw
   Fe(2)     4.921e-3
   Cl        10e-3
SURFACE 1
         Hfo_sOH        1.17e-5    213.    0.596
         Hfo_wOH        4.67e-4
-sites_units density
   SurfgoeOH 1.68 17.5 0.354
-sites_units density
   SurfmagOH 2.05 36.4 0.02

EQUILIBRIUM_PHASES 1
   Fix_H+ -6.5 HCl
END

#----------------------------------------------------------------
# t2 A
SOLUTION 1
   pH        6.5
   units     mol/kgw
   Fe(2)     4.646e-3
   Cl        10e-3
SURFACE 1
         Hfo_sOH        1.06e-5    213.    0.541
         Hfo_wOH        4.23e-4
-sites_units density
   SurfgoeOH 1.68 17.5 0.356
-sites_units density
   SurfmagOH 2.05 36.4 0.082

EQUILIBRIUM_PHASES 1
   Fix_H+ -6.5 HCl
END
```

S12.5 Comparison between modeled and measured H^+ release during ferrihydrite transformation

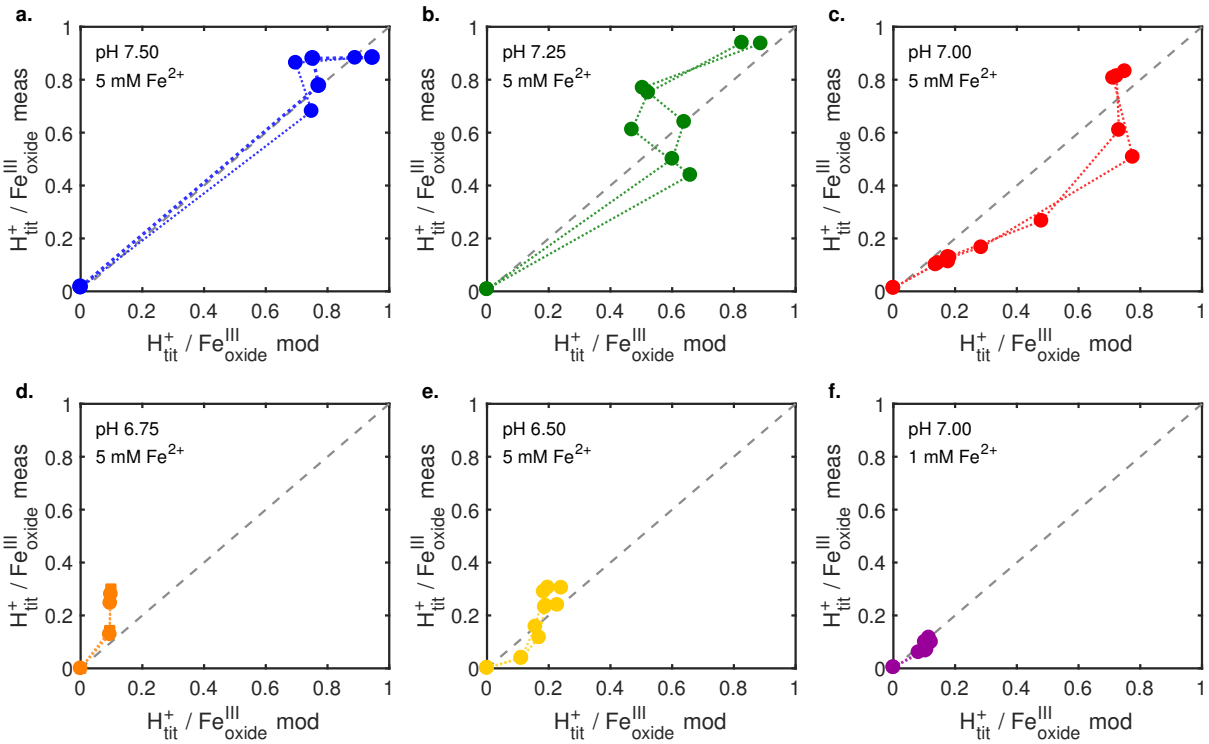

Figure S22 Comparison between H^+ release and changes in iron oxide mineralogy. $H^+_{tit}/Fe^{III}_{oxide}$ values measured in pH-stat titration (labelled '$H^+_{tit}/Fe^{III}_{oxide}$ meas') are plotted versus $H^+_{tit}/Fe^{III}_{oxide}$ values modeled ('$H^+_{tit}/Fe^{III}_{oxide}$ mod') based on the molar fractions of Fe^{III} in magnetite and magnetite stoichiometries and considering H^+ displacement from iron oxide surfaces due to Fe^{2+} adsorption and decreasing iron oxide specific surface area.

S13 Electron microscopy imaging

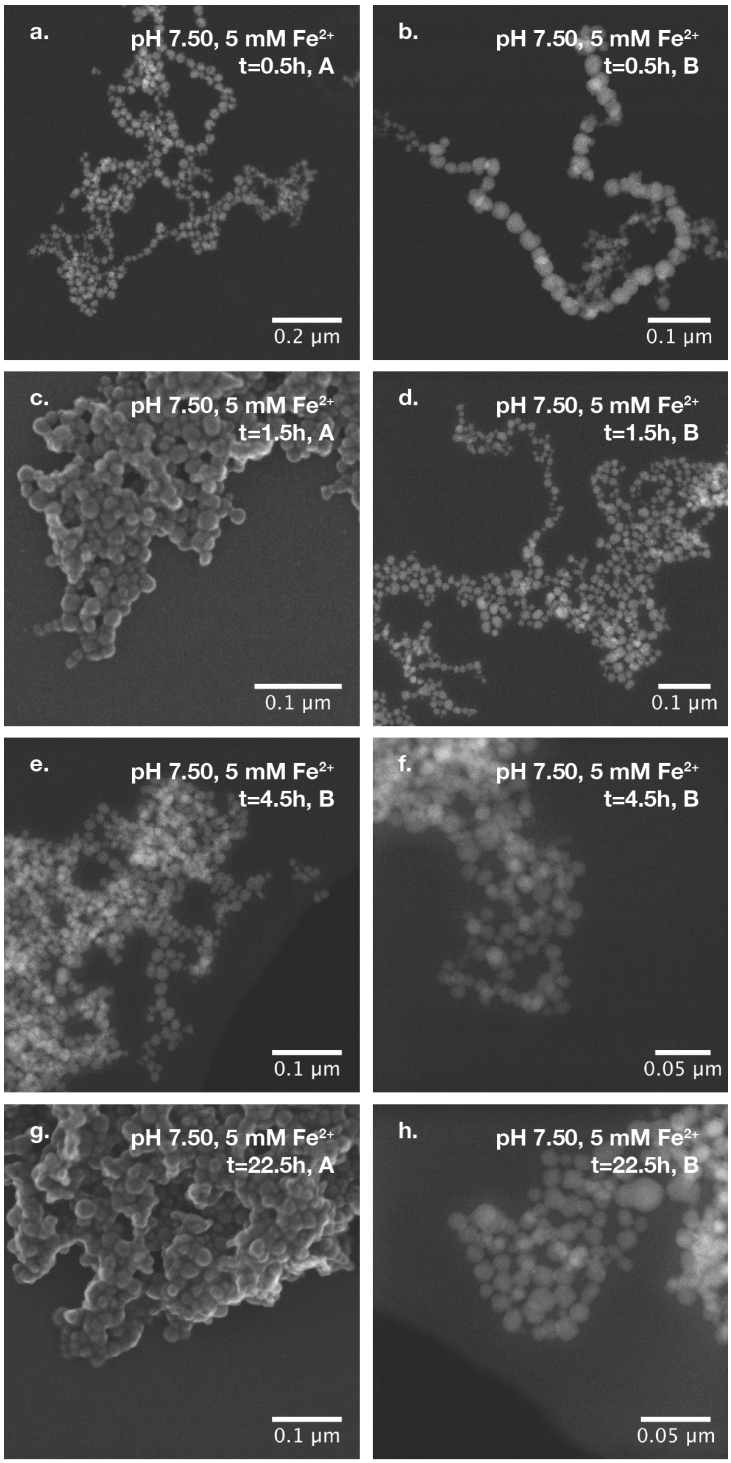

Figure S23 Selected electron microscopy images obtained during ferrihydrite transformation at pH 7.50 and an initial Fe^{2+} concentration of 5 mM. Iron oxide suspensions for electron microscopy analysis were extracted from duplicate reactors A and B at selected time points as indicated on the images. Images were recorded using secondary electron (SE, c., g.) or a high angular annular dark field (HAADF, remaining panels) detector.

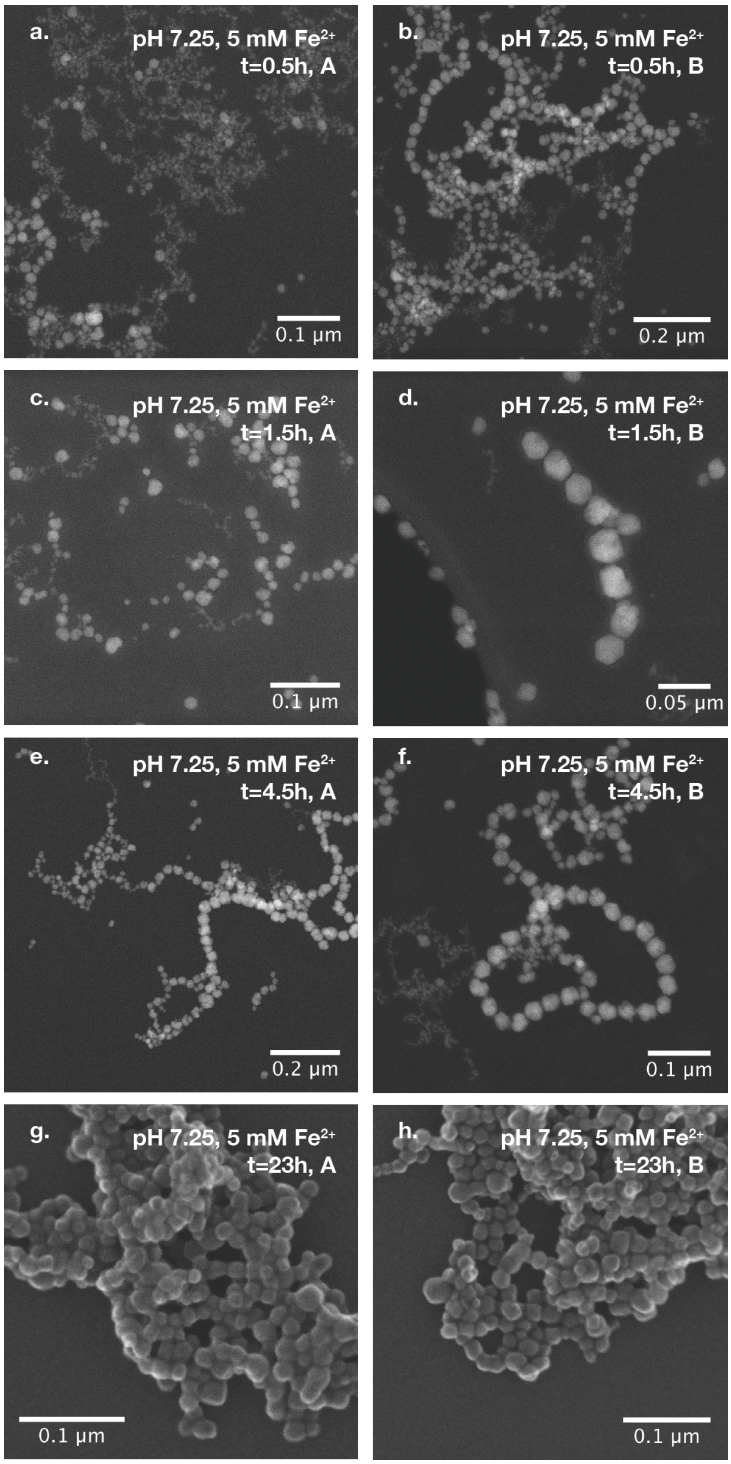

Figure S24 Selected electron microscopy images obtained during ferrihydrite transformation at pH 7.25 and an initial Fe^{2+} concentration of 5 mM. Iron oxide suspensions for electron microscopy analysis were extracted from duplicate reactors A and B at selected time points as indicated on the images. Images were recorded using secondary electron (SE, g., h.) or a high angular annular dark field (HAADF, remaining panels) detector.

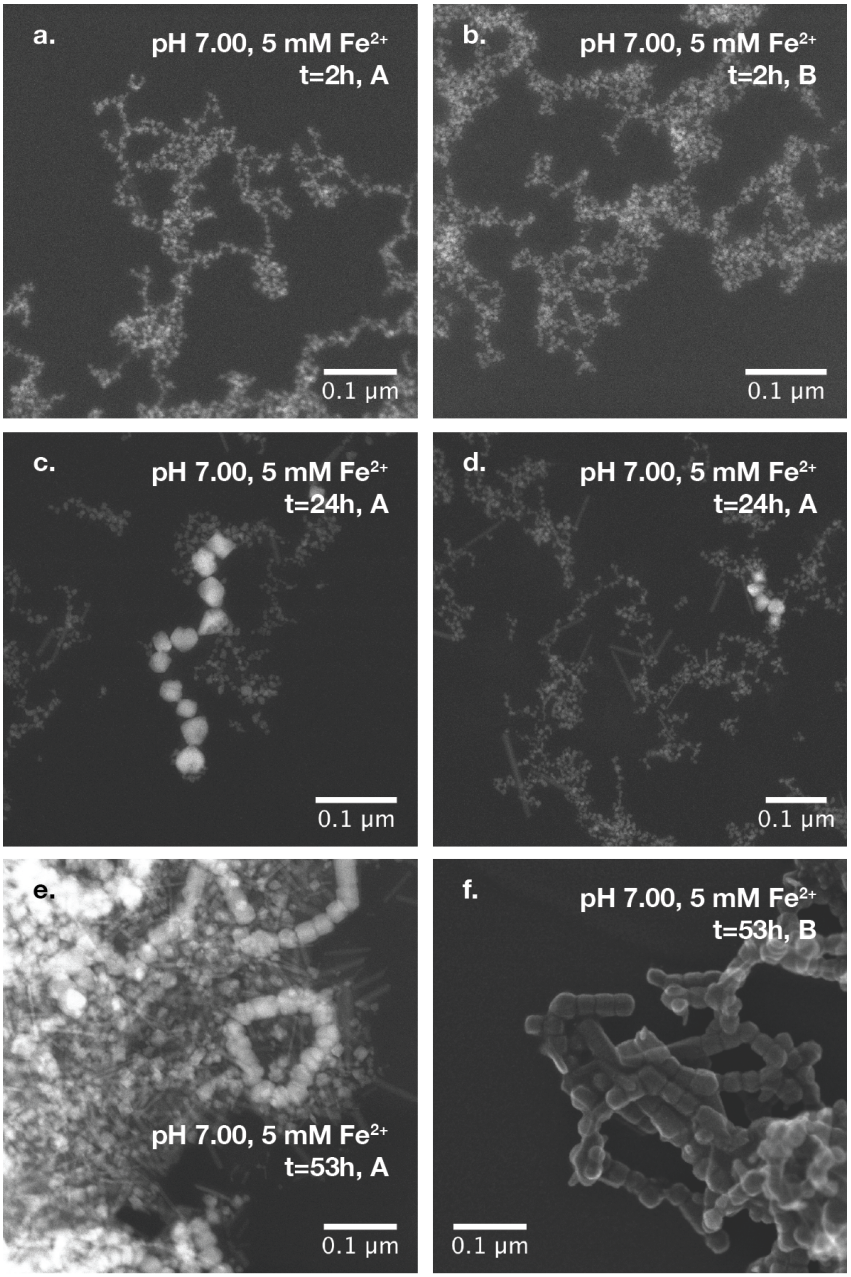

Figure S25 Selected electron microscopy images obtained during ferrihydrite transformation at pH 7.00 and an initial Fe^{2+} concentration of 5 mM. Iron oxide suspensions for electron microscopy analysis were extracted from duplicate reactors A and B at selected time points as indicated on the images. Images were recorded using secondary electron (SE, f.) or a high angular annular dark field (HAADF, remaining panels) detector.

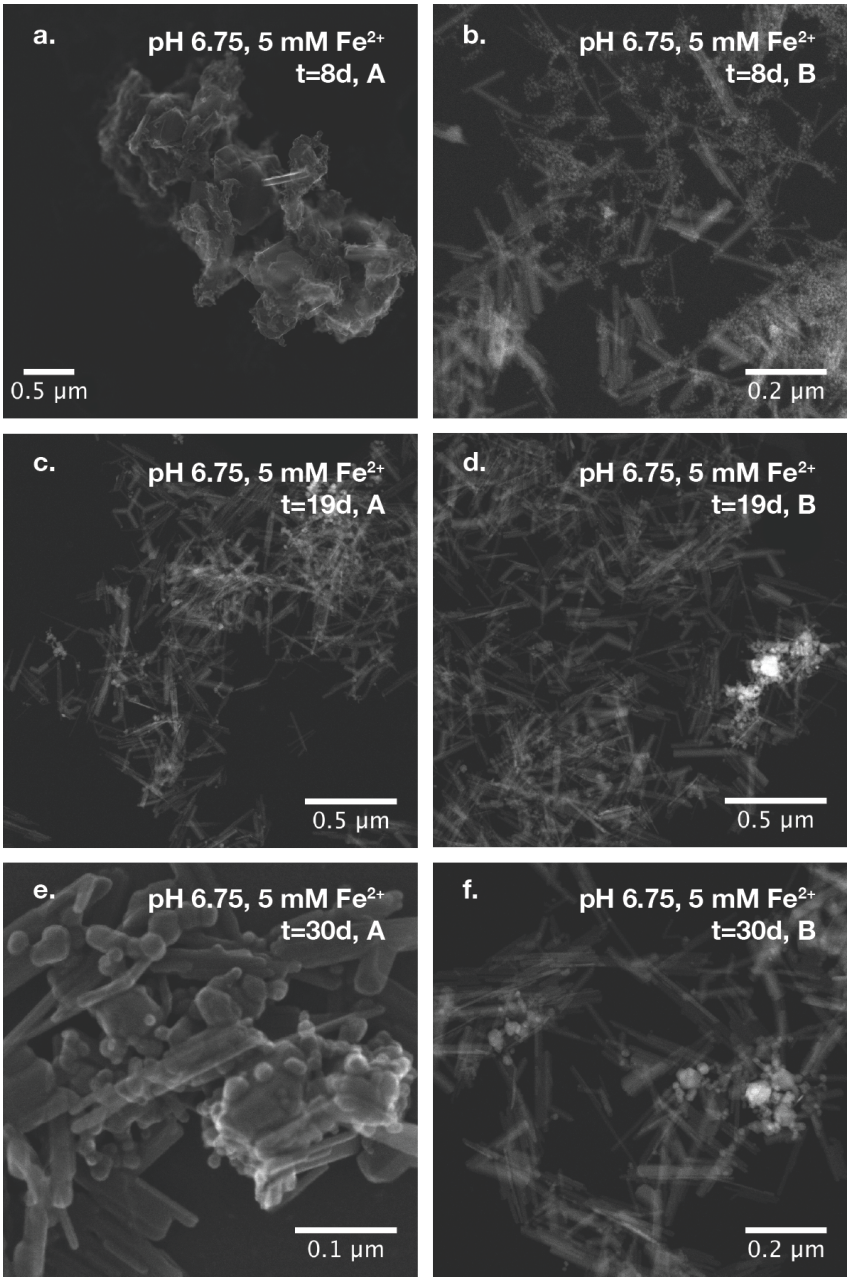

Figure S26 Selected electron microscopy images obtained during ferrihydrite transformation at pH 6.75 and an initial Fe^{2+} concentration of 5 mM. Iron oxide suspensions for electron microscopy analysis were extracted from duplicate reactors A and B at selected time points as indicated on the images. Images were recorded using secondary electron (SE, c., e.) or a high angular annular dark field (HAADF, remaining panels) detector.

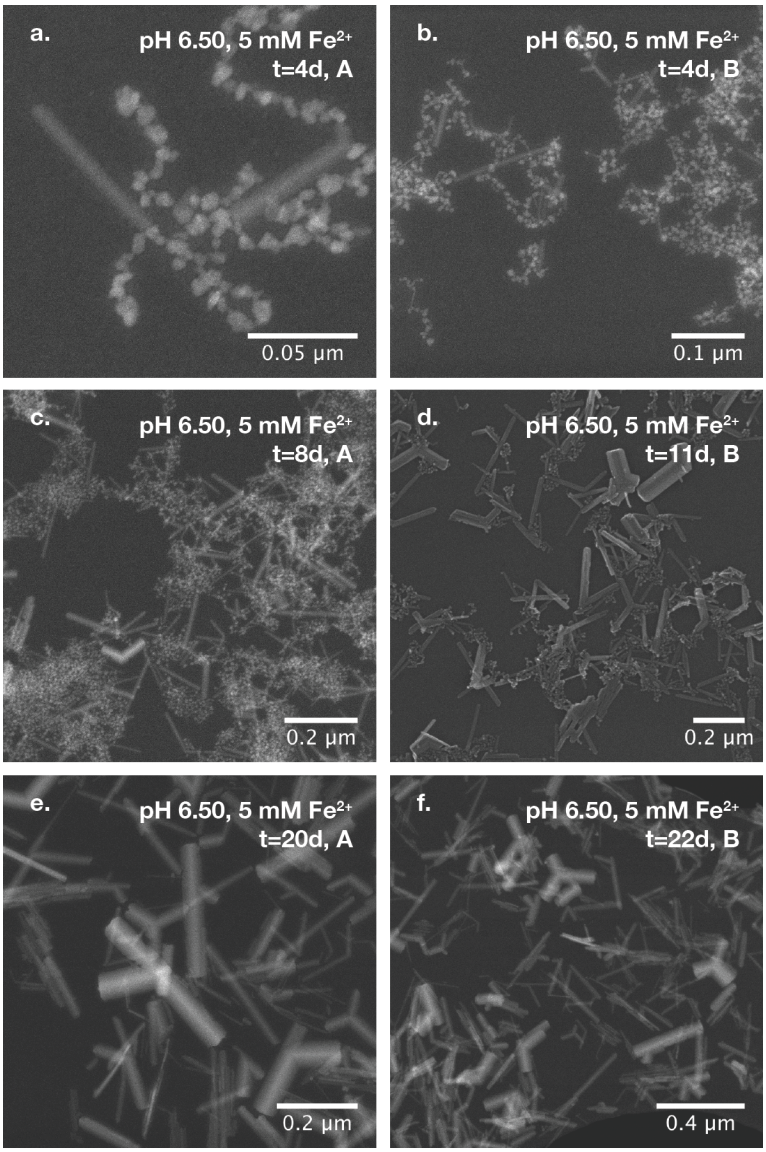

Figure S27 Selected electron microscopy images obtained during ferrihydrite transformation at pH 6.50 and an initial Fe^{2+} concentration of 5 mM. Iron oxide suspensions for electron microscopy analysis were extracted from duplicate reactors A and B at selected time points as indicated on the images. Images were recorded using secondary electron (SE, d.) or a high angular annular dark field (HAADF, remaining panels) detector.

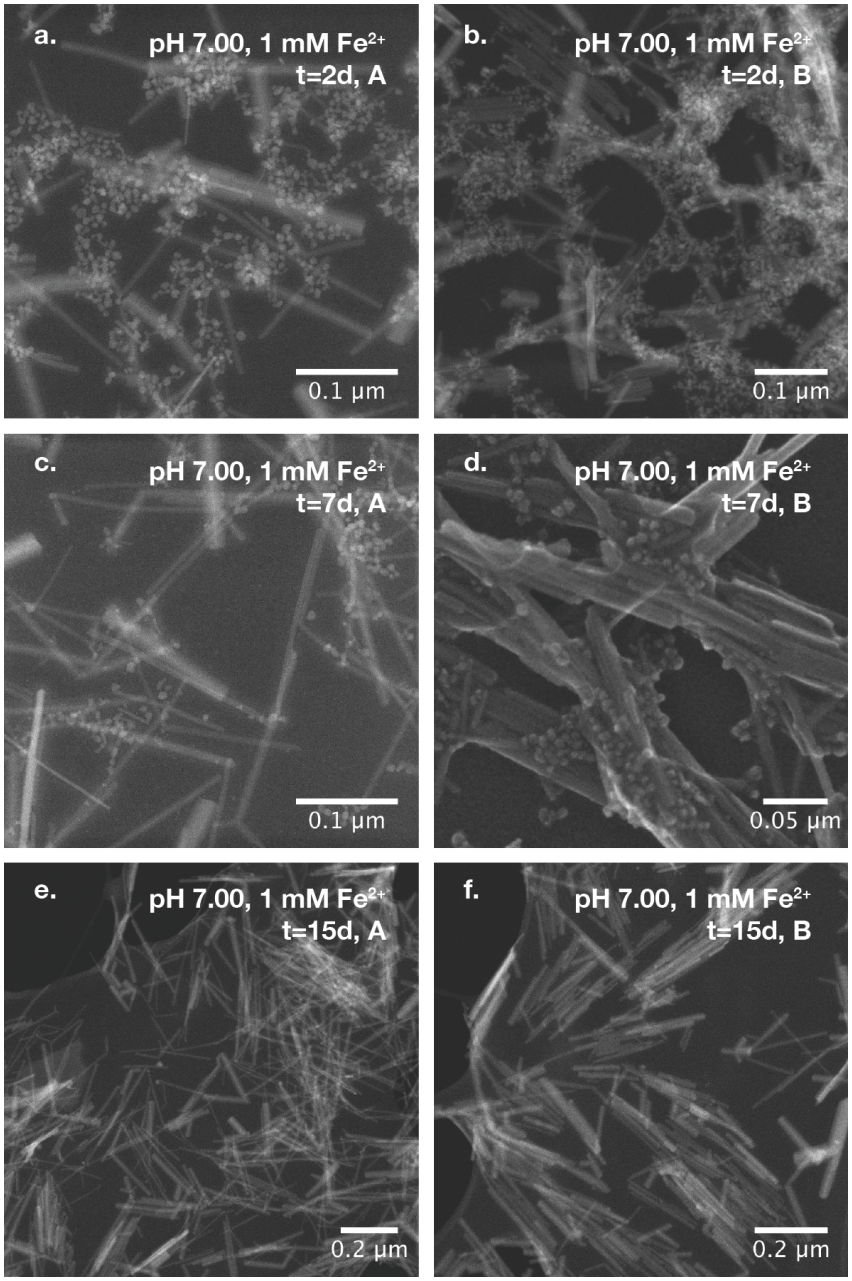

Figure S28 Selected electron microscopy images obtained during ferrihydrite transformation at pH 7.00 and an initial Fe^{2+} concentration of 1 mM. Iron oxide suspensions for electron microscopy analysis were extracted from duplicate reactors A and B at selected time points as indicated on the images. Images were recorded using secondary electron (SE, d.) or a high angular annular dark field (HAADF, remaining panels) detector.

S14 Extents and rates of iron oxide reduction

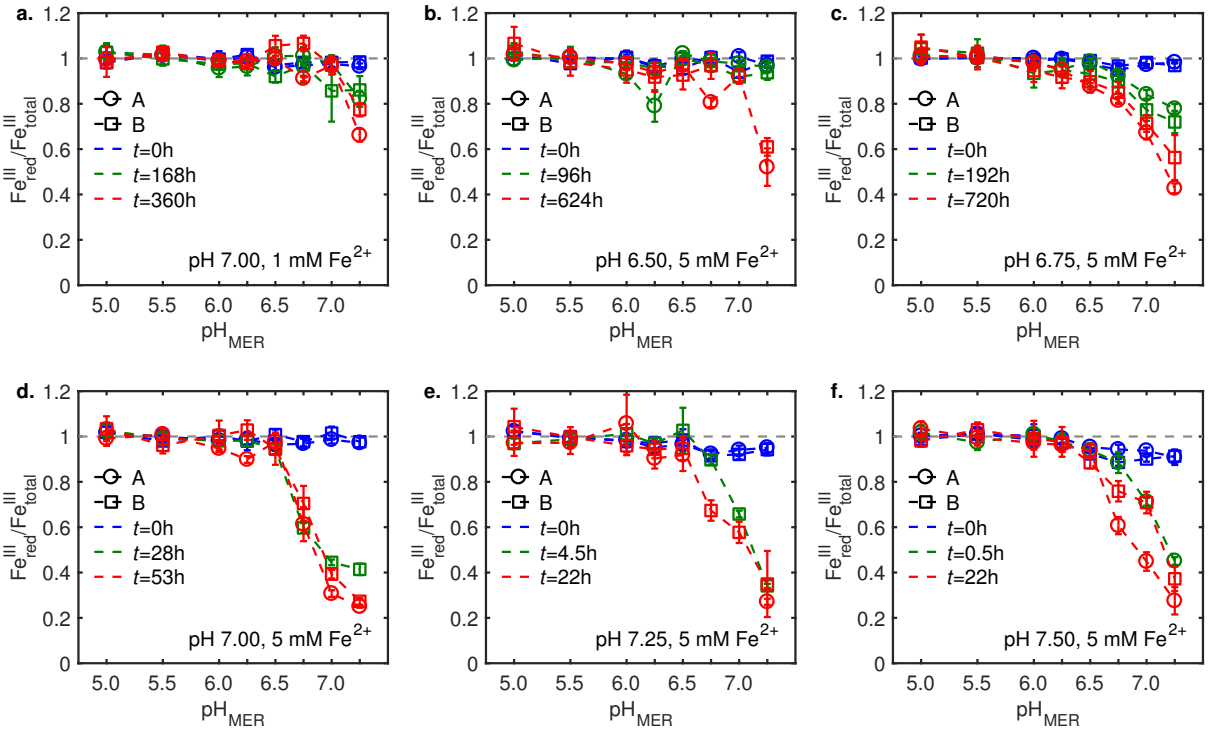

Figure S29 Characterization of the reducible fractions of oxide Fe^{III} ($Fe^{III}_{red}/Fe^{III}_{oxide}$) in MER at pH_{MER} = 5.00 to 7.25, all at E_H^{MER}=−0.35 V, during all ferrihydrite transformation experiments. $Fe^{III}_{red}/Fe^{III}_{oxide}$ values were determined as described in the materials and methods section in the main manuscript. For each transformation experiment, Fe^{III}_{red} /Fe^{III}_{oxide} are shown for three selected time points during the transformation (labelled on the plot) and for duplicate reactors A (circles) and B (squares).

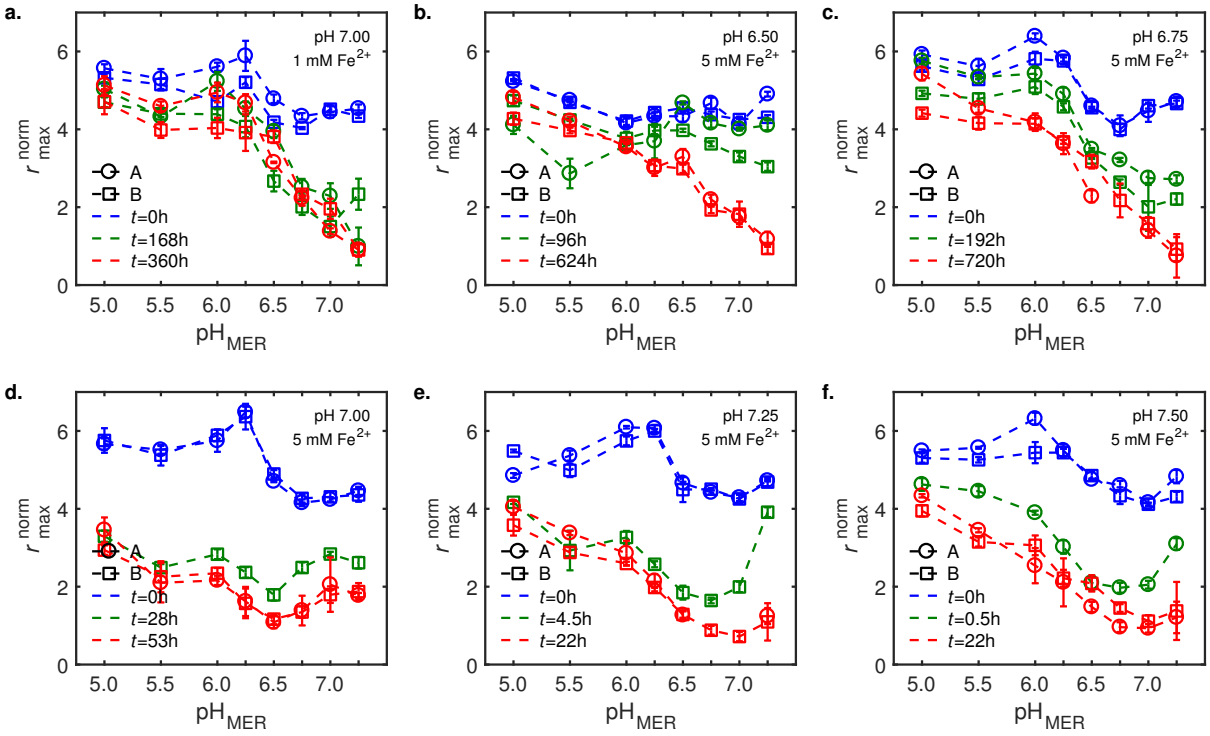

Figure S30 Normalized maximum reduction rates (r_{max}^{norm} [$mmol_{e^-}$ $mol_{Fe^{III}}^{-1}$ s^{-1}]) of iron oxide suspensions in MER at pH_{MER} = 5.00 to 7.25, all at E_H^{MER}=−0.35 V. See materials and methods for the calculation of r_{max}^{norm}. r_{max}^{norm} are shown at three selected time points during each transformation experiment (labelled on the plot) and for duplicate reactors A (circles) and B (squares).

S15 Reference iron oxide reduction extents and rates

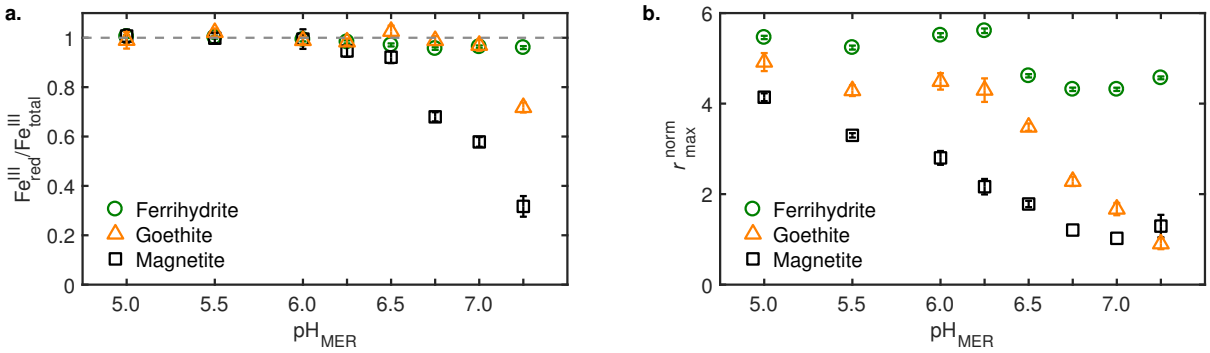

Figure S31 Reducible fractions of Fe^{III} in ferrihydrite, goethite and magnetite and relative maximum reduction rates of ferrihydrite, goethite and magnetite in MER at $E_H^{MER} = -0.35$ V as a function of pH_{MER}. Ferrihydrite data represent the average of the t_0 measurements in all transformation experiments, while goethite data represents the average of the t_{end} measurements in the transformation experiment at pH 7.00 and 1 mM Fe^{2+}, and magnetite data represents the average t_{end} measurements in the transformation experiments at pH 7.25 and 7.50, both at 5 mM Fe^{2+}. Reducible fractions of oxide Fe^{III}, $Fe^{III}_{red}/Fe^{III}_{oxide}$, and normalized maximum reduction rates, r^{norm}_{max} [$mmol_{e^-}$ $mol_{Fe^{III}}{}^{-1}$ s^{-1}], were calculated as described in the materials and methods section in the main manuscript. (r^{norm}_{max} [$mmol_{e^-}$ $mol_{Fe^{III}}{}^{-1}$ s^{-1}], **b.**) The displayed data was used to calculate $Fe^{III}_{red}/Fe^{III}_{oxide}$ and relative R^{max}_{red} in Figures 4 in the main manuscript and Figure S32.

S16 Linking changes in iron oxide reduction extents to mineralogy

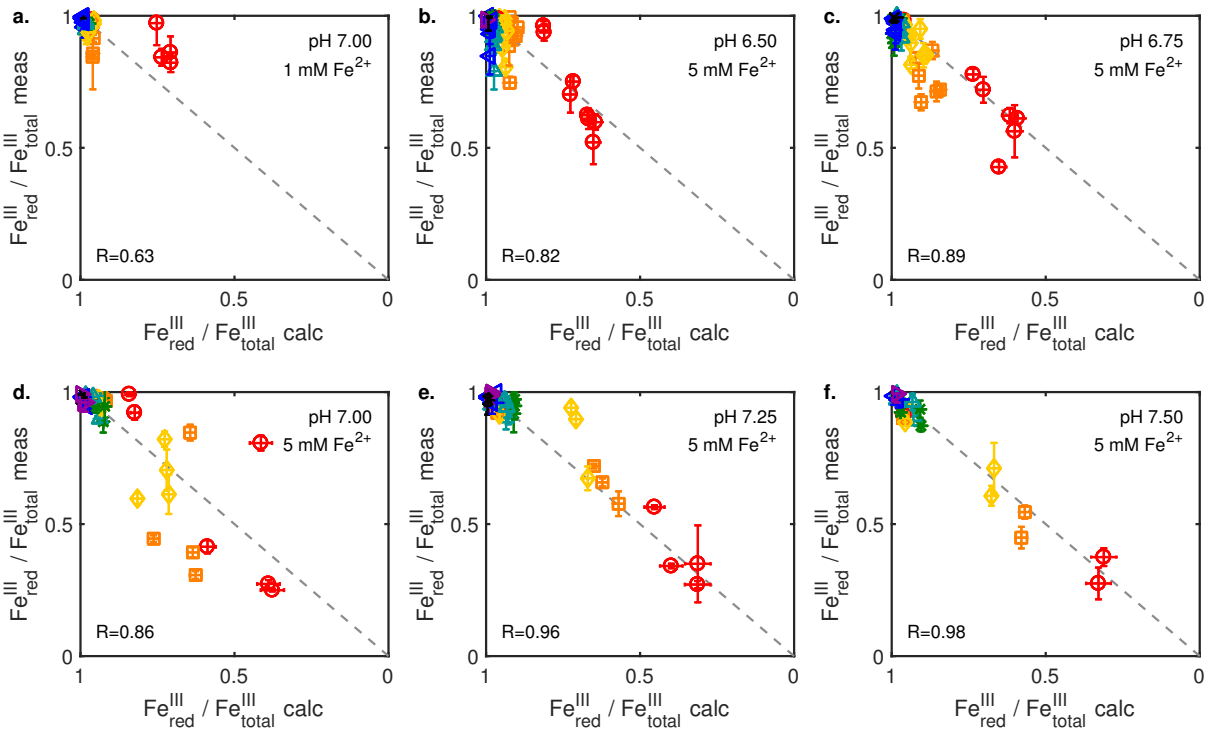

Figure S32 Comparison between changes in the extent of oxide Fe^{III} reduction and iron oxide mineralogy. Measured reducible fractions of oxide Fe^{III} in MER ('Fe^{III}_{red} /Fe^{III}_{oxide} meas') are plotted versus modeled reducible fractions of oxide Fe^{III} in MER ('Fe^{III}_{red} /Fe^{III}_{oxide} mod') based on iron oxide mineralogy (see main manuscript). Data were obtained at or calculated for pH_{MER}=5.00 (x), 5.50 (right-pointing triangle), 6.00 (left-pointing triangle), 6.25 (triangle), 6.50 (star), 6.75 (diamonds), 7.00 (squares), 7.25 (circles) (all at $E_H^{MER} = -0.35$ V). A Pearson correlation analysis was performed separately for each transformation experiment and correlation coefficients (R) are given on the plots (see Table S6 for additional details).

Table S6 Statistical analysis of the measured and modeled reducible fractions of oxide Fe^{III} in MER in Figure S32. A Pearson correlation analysis was performed separately for each transformation experiment. The number of data points (N), the Pearson correlation coefficient (R) with lower and upper bounds (R lower/upper bound) and P value are given.

pH	Initial Fe^{2+} (mM)	N	R	R lower bound	R upper bound	P
6.50	5	80	0.8188	0.7298	0.8805	3.06E-20
6.75	5	64	0.8929	0.8291	0.9338	3.68E-23
7.00	5	64	0.8636	0.7842	0.9151	4.26E-20
7.25	5	48	0.9585	0.9258	0.9770	1.31E-25
7.50	5	48	0.9740	0.9539	0.9854	2.50E-31
7.00	1	64	0.7473	0.6143	0.8390	1.32E-12

Table S7 Statistical analysis of the measured and modeled reducible fractions of oxide Fe^{III} in MER in Figure 4 in the main manuscript. A Pearson correlation analysis was performed separately for each transformation experiment. The number of data points (N), the Pearson correlation coefficient (R) with lower and upper bounds (R lower/upper bound) and P value are given.

pH	Initial Fe^{2+} (mM)	N	R	R lower bound	R upper bound	P
6.50	5	80	0.7963	0.6988	0.8647	1.06E-18
6.75	5	64	0.9647	0.9422	0.9786	4.56E-37
7.00	5	64	0.7580	0.6295	0.8462	4.09E-13
7.25	5	48	0.8660	0.7690	0.9240	7.82E-15
7.50	5	48	0.9859	0.9749	0.9921	2.14E-37
7.00	1	64	0.9662	0.9447	0.9794	3.42E-38

References

[1] Schwertmann, U., and Cornell, R. M. *Iron Oxides in the Laboratory: Preparation and Characterization*, 2nd ed.; Second, Completely Revised and Extended Ed.; Wiley-VCH: Weinheim, 2000.

[2] Tamura, H., Goto, K., Yotsuyanagi, T., and Nagayama, M. (1974) Spectrophotometric determination of iron(II) with 1,10-phenanthroline in the presence of large amounts of iron(III). *Talanta 21*, 314–318.

[3] Scarlett, N. V. Y., and Madsen, I. C. (2006) Quantification of phases with partial or no known crystal structures. *Powder Diffr. 21*, 278–284.

[4] Gorski, C. A., and Scherer, M. M. (2010) Determination of nanoparticulate magnetite stoichiometry by Mössbauer spectroscopy, acidic dissolution, and powder X-ray diffraction: A critical review. *Am. Mineral. 95*, 1017–1026.

[5] Parkhurst, D. L., and Appelo, C. A. J. *USGS - Description of input and examples for PHREEQC Version 3—A computer program for speciation, batch-reaction, one-dimensional transport, and inverse geochemical calculations*; 2013.

[6] Liger, E., Charlet, L., and Van Cappellen, P. (1999) Surface catalysis of uranium(VI) reduction by iron(II). *Geochim. Cosmochim. Acta 63*, 2939–2955.

[7] Mayant, C., Grambow, B., Abdelouas, A., Ribet, S., and Leclercq, S. (2008) Surface site density, silicic acid retention and transport properties of compacted magnetite powder. *Phys. Chem. Earth A/B/C 33*, 991–999.

[8] Appelo, C. A. J., Van Der Weiden, M. J. J., Tournassat, C., and Charlet, L. (2002) Surface complexation of ferrous iron and carbonate on ferrihydrite and the mobilization of arsenic. *Environ. Sci. Technol. 36*, 3096–3103.

[9] Dixit, S., and Hering, J. G. (2006) Sorption of Fe(II) and As(III) on goethite in single- and dual-sorbate systems. *Chem. Geol. 228*, 6–15.

[10] Aeppli, M., Voegelin, A., Gorski, C. A., Hofstetter, T. B., and Sander, M. (2018) Mediated electrochemical reduction of iron (oxyhydr-)oxides under defined thermodynamic boundary conditions. *Environ. Sci. Technol. 52*, 560–570.

[11] Fischer, W. R. (1987) Standard potentials (E_0) of iron(III) oxides under reducing conditions. *Z. Pflanzenernähr. Bodenkd. 150*, 286–289.

[12] Gorski, C. A., Edwards, R., Sander, M., Hofstetter, T. B., and Stewart, S. M. (2016) Thermodynamic characterization of iron oxide-aqueous Fe^{2+} redox couples. *Environ. Sci. Technol. 50*, 8538–8547.

[13] Pang, S. C., Chin, S. F., and Anderson, M. A. (2007) Redox equilibria of iron oxides in aqueous-based magnetite dispersions: Effect of pH and redox potential. *J. Colloid Interface Sci. 311*, 94–101.

[14] Gorski, C. A., Nurmi, J. T., Tratnyek, P. G., Hofstetter, T. B., and Scherer, M. M. (2010) Redox behavior of magnetite: Implications for contaminant reduction. *Environ. Sci. Technol. 44*, 55–60.